REVISED MODELS FOR ATTENUATION OF MODIFIED MERCALLI INTENSITY IN NEW ZEALAND EARTHQUAKES

D. J. Dowrick[1, 2] and D. A. Rhoades[1, 3]

SUMMARY

This paper presents simple two-dimensional models for attenuation of Modified Mercalli intensity in New Zealand earthquakes, which improve upon the models published by the present authors in 1999. First, the models now ensure that the attenuation functions in the two orthogonal directions converge to the same value at zero source distance. Secondly, an improved fit has been achieved through a modification of the algebraic form of the log distance term in the attenuation function. An additional improvement is the completion of the attenuation model for Deep events ($h_c \geq 70$ km) in the subducting Pacific plate, which was not fully dealt with in our previous paper. Intensity saturation effects are demonstrated. A comparison is made between our New Zealand model and one for the intraplate region of South China where the attenuation rate is considerably lower.

1.0 INTRODUCTION

In 1999, the authors published the results of a study (Dowrick and Rhoades, 1999) on the attenuation of Modified Mercalli (MM) intensity in New Zealand earthquakes, which represented an advance in data and modelling compared with previous New Zealand studies, e.g. Dowrick (1992) and Smith (1995). The biggest difficulty with attenuation modelling is in adequately modelling the near-source zones of large shallow earthquakes. This difficulty arises partly because of the scarcity of good quality data for such zones, and partly because of the inherent limitations of tractable attenuation functions.

Our 1999 study did not resolve the near-source-modelling difficulty as well as was desirable. One unsatisfactory aspect was that the independently fitted models in the along-strike and normal-to-strike directions were not constrained to converge to the same value at zero distance from the source. Another problem was encapsulated in the large difference between the sizes of the isoseismals of two of the largest earthquakes (1929 Murchison and 1931 Hawke's Bay), although they were of similar magnitude (M_W 7.7 and 7.8) and were both classified as reverse faulting focal mechanisms. Subsequently, a study of the 1931 Hawke's Bay earthquake has found it to be predominantly strike-slip rather than reverse (Doser and Webb, 2003). The potential of this solitary finding to improve near source modelling of the data was immediately recognised. These matters have been addressed here, in conjunction with a small modification to the functional form of the model.

[1] *Institute of Geological & Nuclear Sciences, Lower Hutt*
[2] *Fellow*
[3] *Member*

2.0 EARTHQUAKES STUDIED

In all, 89 earthquakes from the period 1855-1998 inclusive are taken into account, as listed in Table 1. These events comprise the 85 earthquakes of our 1999 data set, plus the 1994 Arthur's Pass earthquake (No. 86), the 1995 Cass earthquake (No. 88), the 1921 Hawke's Bay earthquake (No. 7), and the 1945 Puysegur earthquake (No. 27).

As seen in Figure 1, the earthquakes are distributed mainly along the eastern part of the North Island, the northern part of the South Island, and the western part of the South Island, associated with the boundary of the Pacific and Australian tectonic plates. Ten events provide data on attenuation in the Taupo Volcanic Zone (TVZ) (Figure 1 and Table 1). Of the 89 events in our data set, 12 were in the dipping slab of the subducting Pacific plate at depths of 72-300 km.

In the data set there are 54 Crustal events, 5 Interface events, 18 dipping slab events with $h_c \leq 60$ km, and 12 deeper slab events, respectively denoted C, I, S_{60} and S_D in Table 1. In addition to these real earthquakes, two dummy events (Nos. 90, 91) were introduced to help control the near source modelling of large shallow events in the volcanic region for which little real data exists, and crustal events with normal focal mechanisms. The largest event in the TVZ is the M_W 6.5 1987 Edgecumbe earthquake, which is a difficult event to model appropriately because its fault rupture was on the southeast boundary of the TVZ.

Information defining source mechanisms is given (Table 1) in two forms, namely rake angle γ, and the three common geological descriptors, normal (N), strike-slip (S) and reverse (R). Rake is the direction of slip in the fault plane, where the angles 0° and 180° represent horizontal movement (pure S), while 90° and 270° correspond to pure R and pure N respectively. The mechanisms N, S, R given in Table 1 are the predominant mechanisms, which are defined as follows. S corresponds to γ in the ranges 315° - 045° and 135° - 225° ; R to γ in the range 46° - 134°; and N to γ in the range 226° - 314°. The crustal events comprise 11 R, 22 S, 19 N and one unknown mechanism. The shallow ($h_c \leq 60$ km) slab events comprise two R, two S, 14 N and one unknown mechanism, while there are three R and two S Interface earthquakes.

3.0 INTENSITY AND DISTANCE DATA

As in our previous study (Dowrick and Rhoades, 1999) the geometry of the isoseismals is measured in relation to fault strike. As shown in Figure 2, the dimensions of the isoseismals of all earthquakes other than Deep Pacific Slab events are defined as:

a = horizontal radius along the fault strike;

b = horizontal radius normal to strike;

r_a , r_b = source (-to-isoseismal) distances corresponding to a, b, such that for example:

$$r_a = (a^2 + h_f^2)^{1/2} \quad (1)$$

where h_f = depth to top of fault rupture.

The corresponding geometry for Deep Pacific Slab events is shown in Figure 3. The isoseismal patterns for these events differ from the others in two respects. First, they are asymmetrical about their effective strike line, and secondly, they all share the same effective strike line (defined as line AA on Figure 1). The asymmetry is dealt with by measuring the lateral dimensions of the isoseismals in two opposite directions normal to line AA, such that:

b_e = horizontal radius normal to AA in the direction approximately ESE, and

b_w = horizontal radius normal to AA in the direction approximately WNW.

As discussed by Dowrick and Rhoades (1999), the effective surface strike of the Deep earthquakes is constrained by the highly attenuating mantle wedge above the dipping slab, to be in approximately the same location for all Deep Pacific Slab events. This generalisation is true not only for the Deep events in our data set, but also for most of the 17 other Deep events in the Atlas of isoseismal maps (Downes, 1995), which were excluded from this study because no estimates of M_W were available. The line AA corresponds closely to the 35 km depth contour on the top of the dipping slab as defined by Ansell and Bannister (1996). This depth corresponds approximately to the separation point between the Australian and Pacific plates. Line AA passes through Lottin Point (near Cape Runaway) and Cape Koamaru (on Arapawa Island).

Table 1: **Source parameters of earthquakes considered in this study.**
(See explanatory notes at foot of table).

No	Date	Time	°S	°E	h	h_c	h_t	M_W	M_s	T	FM	Rn	θ	β	γ
1	1855 Jan 23	0932	41.40	175.00	sha	19	0	8.2C	-	C	S	M	45	90	180
2	1888 Aug 31	1645	42.60	172.40	sha	8	0	7.1C	7.1	C	S	M	80	90	180
3	1901 Nov 15	2015	42.70	173.30	12	10	4	6.78B	6.87	C	R?	M	50	70	90
4	1911 Oct 5	0736	39.50	177.00	25?	25	23	5.56B	5.32	S_{60}	N	M	40	45	270
5	1912 May 26	0635	38.00	175.00	cru	15	12	5.65B	5.52	C	N	M	0	45	270
6	1914 Nov 22	0814	37.50	176.50	300	300	300	7.29B	6.46	S_D	U	D	40	U	U
7	1921 Jun 28	1358	39.30	176.40	80	76	72	6.60B	6.41	S_D	U	D	40	U	U
8	1922 Jul 4	0515	38.60	176.10	v.sh	3	0	4.93B	4.39	C	N	V	35	45	U
9	1922 Jul 14	0356	38.60	176.10	v.sh	3	0	5.12B	4.73	C	N	V	35	45	U
10	1922 Sep 5	0233	38.60	176.10	v.sh	3	0	5.37B	5.14	C	N	V	35	45	U
11	1922 Dec 25	0333	43.00	173.00	10?	20	15	6.79B	6.42	C	S	M	72	70	170
12	1926 Nov 11	2251	37.70	175.50	sha	5	3	4.6D	-	C	N	M	340	45	270
13	1929 Mar 9	1050	42.80	171.90	15?	11	0	6.95B	7.05	C	S	M	65	90	178
14	1929 May 7	1614	40.00	175.50	cru	10	8	5.45B	5.22	C	S	M	32	90	180
15	1929 Jun 16	2247	41.70	172.20	15?	9	0	7.72B	7.79	C	R	M	5	45	69
16	1931 Feb 2	2246	39.30	177.00	30	15	3	7.79B	7.83	C	R	M	40	70	165
17	1932 May 5	0823	39.60	176.90	25?	20	17	5.95B	5.87	S_{60}	N	M	40	45	270
18	1932 Sep 15	1355	38.90	177.60	30?	8	2	6.79B	6.87	C	S	M	56	85	180
19	1934 Mar 5	1146	40.51	176.29	12	8	0	7.36B	7.56	C	S	M	40	82	180
20	1934 Mar 15	1046	39.31	177.17	10	25	20	6.38B	6.37	S_{60}	S	M	35	86	178
21	1938 Dec 15	0912	40.00	177.00	30?	25	22	5.76B	5.61	S_{60}	N	M	36	45	270
22	1938 Dec16	1721	45.00	167.00	60	47	40	7.06B	7.05	S_{60}	R	M	117	88	72
23	1942 Jun 24	1116	40.90	175.90	15	12	4	7.07B	7.16	C	S	M	35	86	170
24	1942 Aug 1	1234	41.00	175.80	43	40	35	6.96B	6.97	S_{60}	N	M	28	80	-67
25	1943 Feb 17	0215	45.19	167.04	33R	36	32	6.37B	6.33	S_{60}	S	M	50	52	15
26	1943 Aug 2	0046	46.27	166.72	31R	31	27	6.57B	6.58	C	S	M	34	53	174
27	1945 Sep 1	2244	46.83	165.80	12R	28	21	6.98B	7.02	C	S	M	35	82	160
28	1946 Feb 12	0616	39.79	174.85	132	132	132	5.77B	5.14	S_D	U	D	40	U	U
29	1946 Jun 26	1234	43.46	171.26	12R	9	5	6.32B	6.37	C	S	M	44	89	180
30	1948 May 22	1921	42.48	172.99	12R	4	1	6.36B	6.43	C	S	M	60	90	177
31	1951 Jan 10	1915	42.79	173.18	12R	10	7	5.93B	5.89	C	R?	M	30	45	90
32	1951 Feb 10	0327	40.21	177.04	33R	20	15	6.21B	6.20	S_{60}	N	M	35	45	270
33	1951 Apr 23	0650	37.53	177.84	80R	80	76	5.99B	5.65	S_D	U	D	40	U	U
34	1951 Jun 24	0441	39.46	176.20	33R	25	23	5.51B	5.25	C	S?	M	27	U	180
35	1952 Aug 28	1040	39.99	176.96	12R	30	26	6.01B	5.91	S_{60}	U	M	35	U	U
36	1953 Jul 4	0207	38.86	175.68	12R	5	3	5.28B	4.99	C	N	VM	0	45	270
37	1956 Jan 30	0843	37.10	177.42	12R	6	0	6.34B	6.37	C	N	V	35	65	U
38	1956 Mar 2	2243	38.90	175.80	12R	5	3	5.0D	-	C	N	V	U	45	U
39	1957 Feb 22	0030	39.19	175.14	5R	15	13	5.25B	4.88	C	N	M	35	45	270
40	1957 Aug 11	0512	39.05	175.97	99	99	96	5.52B	4.90	S_D	U	D	40	U	U
41	1958 Jan 31	0632	39.85	176.58	12R	23	22	5.42B	5.12	I	R	M	36	45	90
42	1959 May 22	0657	41.07	174.30	33R	40	40	5.29B	4.83	C	U	M	40	30	U
43	1960 Feb 3	0221	37.61	178.04	144	144	144	5.79B	5.11	S_D	U	D	40	U	U
44	1960 May 24	1446	44.17	167.73	50R	9	4	6.46B	6.53	C	N	M	265	67	260
45	1962 Jan 23	0649	38.58	174.80	12R	29	18	5.01B	4.47	C	N	M	0	45	270
46	1962 May 10	0027	41.67	171.44	12R	8	5	5.91B	5.88	C	R	M	55	40	88
47	1962 Oct 15	2336	43.54	169.77	12R	20	18	5.57B	5.36	C	S	M	55	90	180
48	1963 Apr 12	0841	38.71	176.76	12R	20	17	5.82B	5.71	C	S	M	15	90	180
49	1963 Dec 22	1335	35.10	173.50	12R	6	4	4.93B	4.36	C	N	M	64	45	270
50	1964 Mar 8	0135	44.30	167.87	12R	5	2	5.89A	5.80	C	S	M	262	83	147
51	1965 Apr 11	0011	42.74	174.10	12R	16	13	6.09A	5.75	S_{60}	N	M	110	55	297
52	1965 Jun 15	0920	37.90	177.53	33R	50	47	5.62B	5.30	S_{60}	N	M	37	45	270

Table 1 continued:

No	Date	Time	°S	°E	h	h_c	h_t	M_W	M_s	T	FM	Rn	θ	β	γ
53	1965 Dec 8	1805	37.09	177.50	156	156	156	6.11A	-	S_D	U	D	40	U	U
54	1966 Mar 4	2358	38.45	177.91	33R	24	21	5.64A	5.77	I	S	M	35	15	U
55	1966 Apr 23	0649	41.63	174.40	22	19	16	5.75A	5.62	C	R	M	232	66	133
56	1968 May 23	1724	41.76	171.96	15	10	0	7.23A	7.41	C	R	M	27	45	103
57	1968 Sep 25	0702	46.49	166.68	12R	4	0	6.27A	6.15	C	S	M	60	85	182
58	1968 Nov 1	0132	41.62	175.05	33R	25	23	5.35B	4.99	S_{60}	N	M	37	45	270
59	1971 Aug 13	1442	42.13	172.10	12R	9	6	5.70A	5.55	C	S	M	242	83	207
60	1972 Jan 8	2133	37.57	175.69	12R	7	5	5.26B	4.94	C	N	M	335	45	270
61	1973 Jan 5	1354	39.04	175.25	160	149	149	6.57A	6.27	S_D	R	D	40	U	U
62	1974 Sep 20	1948	44.40	167.99	12R	25	23	5.55B	5.30	C	R	M	55	45	90
63	1974 Nov 5	1038	39.65	173.63	12R	17	14	5.44A	5.45	C	S	M	195	41	213
64	1975 Jan 4	2037	40.77	174.67	72	72	70	5.24B	4.56	S_D	U	D	40	U	U
65	1975 Jun 10	1011	40.34	175.93	33R	38	36	5.62A	5.14	C	N	M	250	56	257
66	1976 May 4	1356	44.67	167.45	12R	10	5	6.51A	6.38	C	R	M	48	47	130
67	1976 Oct 27	2057	37.83	176.34	12R	5	3	5.0D	-	C	N	V	20	45	U
68	1976 Dec 5	0457	38.17	175.51	1A	5	3	5.0D	-	C	N	M	335	45	270
69	1977 Jan 18	0541	41.73	174.30	33R	34	30	6.02A	5.93	S_{60}	N	M	213	68	251
70	1977 May 31	1850	37.88	176.81	9	6	4	5.39B	5.15	C	N	V	30	45	U
71	1979 Oct 12	1025	46.69	165.74	12R	12	5	7.23A	7.24	C	R	M	7	24	120
72	1982 Sep 2	1558	39.74	176.93	46	31	29	5.38B	5.02	S_{60}	N	M	35	45	270
73	1983 Dec 14	2056	38.36	176.33	5R	3	1	5.06B	4.62	C	N	V	30	45	U
74	1984 Mar 8	0041	38.31	177.29	75	80	76	5.91A	5.40	S_D	R	D	40	U	U
75	1984 Jun 24	1329	43.60	170.56	5R	13	9	6.12A	6.07	C	S	M	62	83	206
76	1985 Jul 19	1433	38.72	177.30	41	31	28	5.92A	5.90	S_{60}	N	M	213	73	255
77	1987 Mar 2	0142	37.88	176.84	10R	6	0	6.53A	6.62	C	N	VM	49	45	257
78	1988 Jun 3	2327	45.10	167.17	57	60	54	6.69A	6.50	S_{60}	R	M	281	U	U
79	1989 May 31	0554	45.27	166.88	23R	24	20	6.33A	6.26	I	S	M	26	48	U
80	1990 Feb 10	0327	42.25	172.65	13	9	6	5.93A	6.04	C	S	M	55	89	163
81	1990 Feb 19	0534	40.38	176.22	24	27	24	6.23A	6.45	S_{60}	N	M	35	70	316
82	1990 May 13	0423	40.35	176.23	12	13	9	6.37A	6.40	C	R	M	40	40	111
83	1993 Apr 11	0659	39.74	176.52	35	24	22	5.63A	5.54	I	R	M	45	15	U
84	1993 Aug 10	0051	45.21	166.71	5R	16	12	6.81A	6.98	I	R	M	41	28	U
85	1993 Aug 10	0946	38.52	177.87	36	39	30	6.19A	6.17	S_{60}	S	M	354	64	168
86	1994 Jun 18	0325	43.01	171.46	-	6	3	6.71A	-	C	R	M	221	47	112
87	1995 Mar 22	1943	41.05	174.18	90	90	86	5.83A	-	S_D	S	D	40	U	U
88	1995 Nov 24	0619	42.98	171.80	-	6	3	6.25A	-	C	S	M	176	46	44
89	1998 Jul 09	1445	30.75	180.86	U	146	146	6.91A	U	S_D	U	D	U	U	U
90	Dummy A					7	0	7.0A		C	N	M			
91	Dummy B					7	0	7.0A		C	N	V			

Notes:

T = Tectonic Type (C,S_{60},I)
FM = Focal Mechanism (N,R,S)
Rn = Region (D,F,M,N,V)
U = Undefined or Unknown

θ = strike
β = dip
γ = rake

Referring again to Equation 1, the values adopted for h_t are given in Table 1, and the values of *a, b* and *b/a* are given in Tables 2 and 3. The data in Tables 1 and 2 are substantially as they were previously (Dowrick and Rhoades, 1999), with a few revisions and additions. In particular, the isoseismal dimensions for the 1942 June 24 earthquake (M_W 7.1) have been revised (enlarged) since the finalisation of its isoseismal map (Downes *et al.*, 2001).

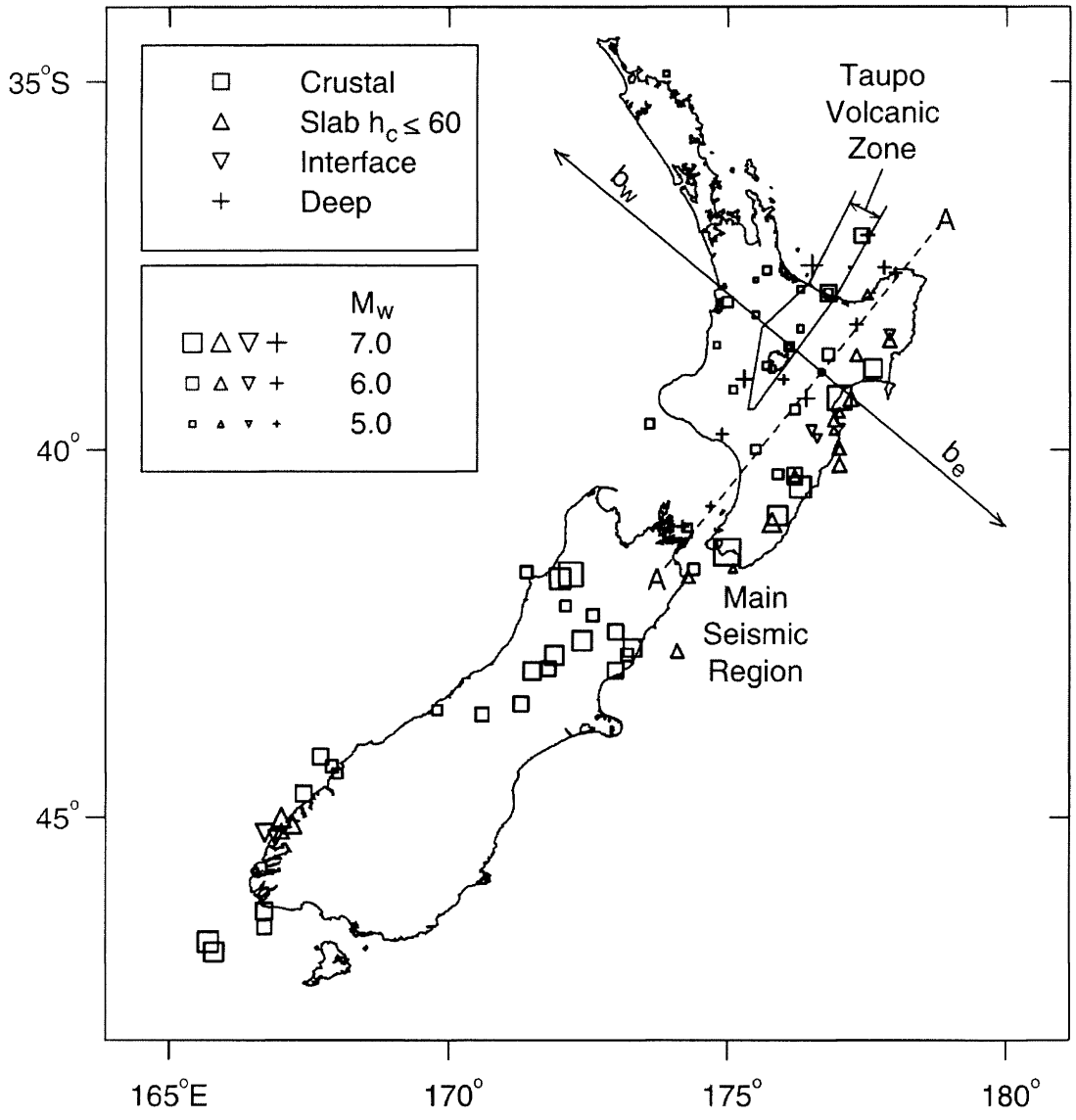

Figure 1: ***Map of locations of earthquakes considered in this study (except Event 88, which is at latitude 30.75 °S). The regions having different attenuation, i.e. the Main Seismic Region and the Taupo Volcanic Zone (TVZ), are indicated, as are events of Crustal, Slab ($h_c \leq 60$ km), Deep (Pacific Slab) ($h_c \geq 70$ km) and Interface origins.***

For modelling the attenuation of Deep events on the east side of line AA, problems arise in obtaining data for b_e (Figures 1 and 3). It is noted that for the Deep events the isoseismals on the east side of line AA in all but two cases lie offshore in the Pacific Ocean, at the point where b_e is measured. As no data exist to constrain these offshore isoseismals directly, their locations offshore were constructed approximately assuming normal attenuation and taking account of the overall shapes of the isoseismals where they cross line AA. This conjecture suffices to ensure that the modelled intensity at the eastern coastline conforms with the intensities as mapped. It is noted that for all the earthquakes in the data set it has been assumed that the source lies vertically below the line of strike, including the Deep events where the offset from line AA is large in some cases (as seen in Figure 1). The simplification of not allowing for the offsets in the distance term causes no observable bias in the fits of the model to the data.

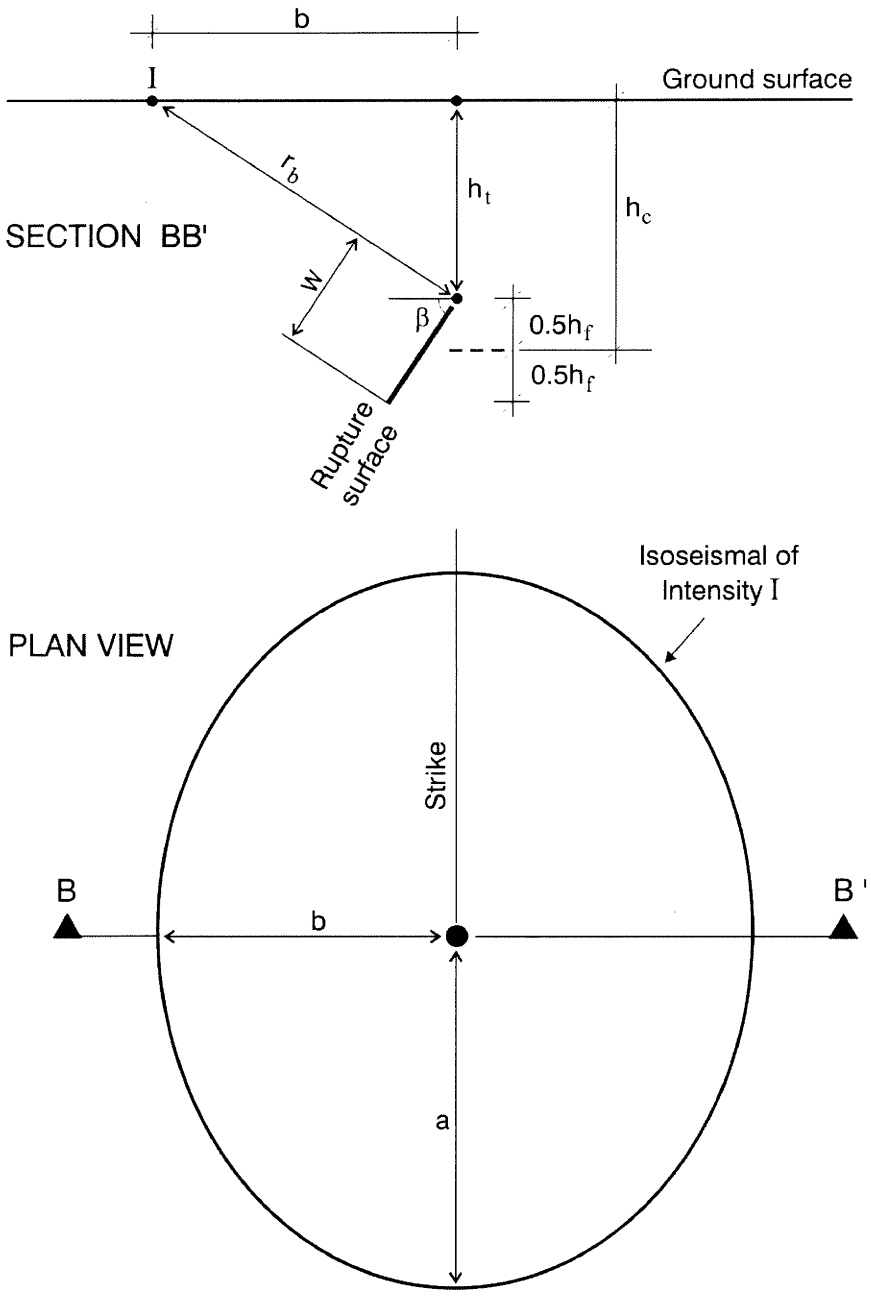

Figure 2: ***Geometry of the isoseismal distance parameters in relation to the source rupture for shallow (h_c < 70 km) earthquakes.***

A further change in our distance data is the revision of the dummy data introduced in our 1999 study to control the near source shape of the attenuation curves, which otherwise predicted spuriously high intensities at the source of shallow (particularly surface rupturing) events. To assist in dealing with this modelling difficulty, a modified distance term has been used, as discussed in Section 4.0.

The dummy data consist of intensities at or near the centre of the isoseismal pattern, designated as I_o. The distances are in the range $1 \leq a \leq 10$ km. The dummy data are identified in Tables 2 and 3 by being in brackets. The intensity I_o was assigned by taking account of near source local observations and the innermost isoseismal intensity (I_{ii}). So as not to excessively perturb the evident near-source attenuation rate

in any given event, I_o was sometimes assigned in half intensity units (e.g. MM7.5), as seen in the Tables 3 and 4 and in Figure 7. In the case of the earthquake of 24 June 1942, the dummy at-source intensity of MM9 is the highest local observation of intensity on its isoseismal map (Downes *et al.*, 2001).

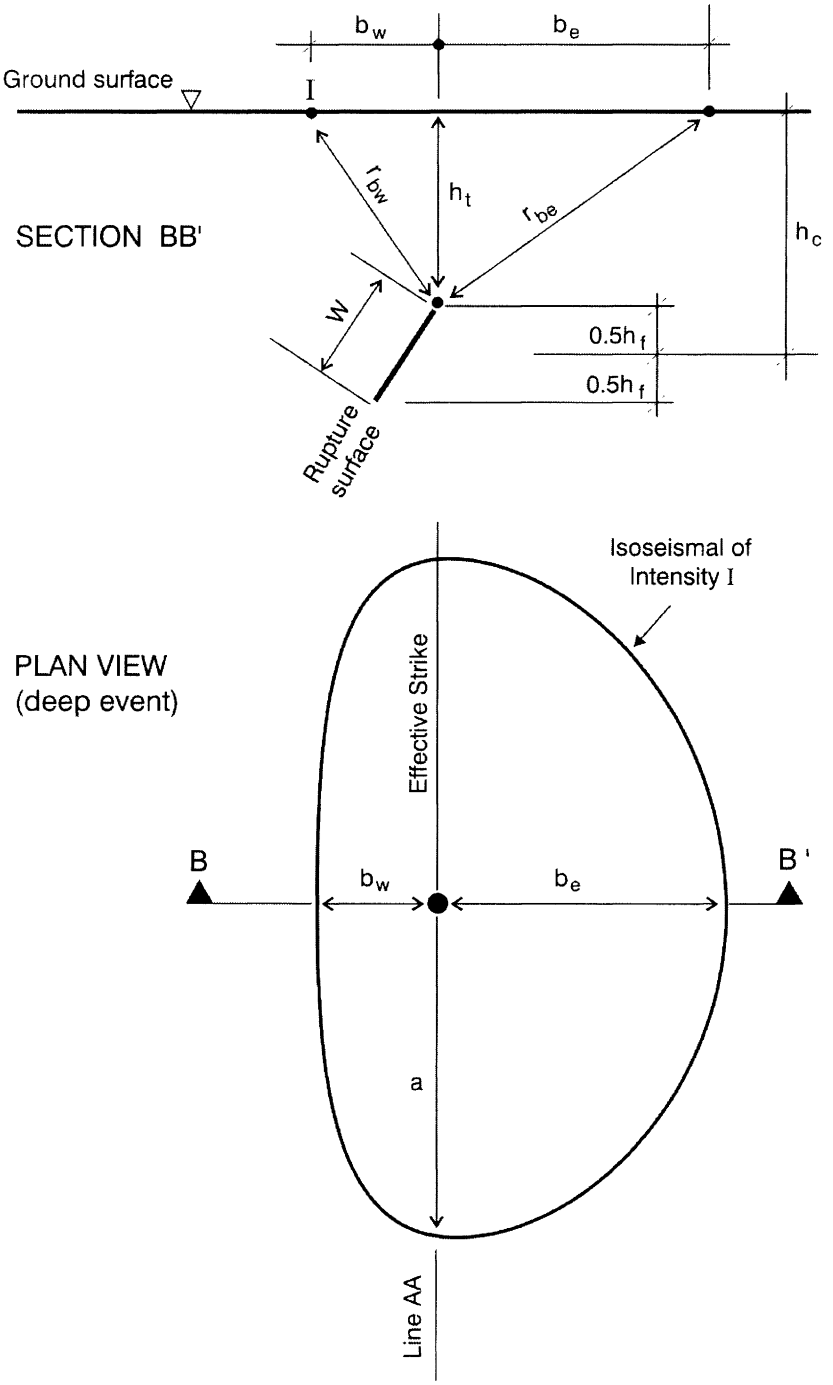

Figure 3: ***Geometry of the isoseismal distance parameters in relation to the source rupture for Deep ($h_c \geq 70$ km) earthquakes in the subducting Pacific plate.***

Table 2: Isoseismal distance data used for shallow earthquakes (see also Table 3).

		MM2			MM3			MM4			MM5			MM6			MM7			MM8			MM9			MM10			MM11		Misc Central Intensities	
MMNo.	Date & Region	*a*	b	b/*a*	*a*	b	b/*a*	*a*	b	b/*a*	*a*	b	b/*a*	*a*	b	b/*a*	*a*	b	b/*a*	*a*	b	b/*a*	*a*	b	b/*a*	a	b	b/a	a	b	a	
1	1855 Jan 23 M													270	244	0.9	204	170	0.8	144	122	0.9	92.5	35	0.4	33	11	0.3	(3)			
2	1888 Aug 31 M											199			105		105	24	0.2	56	16	0.3	21.9	7.8	0.4	(3)						
3	1901 Nov 15 M							256			180	146	0.8	128	80	0.6	64	30	0.5	32	14	0.4	12	4	0.3						(3)	MM9.5
4	1911 Oct 05 M							143	140	1	75	80	1.1	23	18	0.8															(1)	MM6.5
5	1912 May 26 M							192	108	0.6	99	60	0.6	28	26	0.9	(1)															
8	1922 Jul 04 V				58	58	1.0				19	19	1.0				(1)															
9	1922 Jul 14 V				60	60	1.0	45	45	1.0	23	24	1				4	4	1.0													
10	1922 Sep 05 V	80	80	1.0																											(1)	MM7.5
11	1922 Dec 25 M							300			200	150	0.8	120	66	0.6	67	30	0.5	32	12	0.4									(3)	MM8.5
12	1926 Nov 11 M				54	50		29	28	0.97							4	4	1.0													
13	1929 Mar 09 M							300			224	132	0.6	94	66	0.7				34	16	0.5	20	7	0.4	(3)						
14	1929 May 07 M							213	176	0.8	116	98	0.8	60	38	0.6	26	19	0.7	(1)												
15	1929 Jun 16 M										431			281	210	0.8	185	134	0.7	98	68	0.7	50	23	0.46	32	10	0.31	(3)			
16	1931 Feb 02 M							449			315			216	126	0.6	149	77	0.5	101	45	0.4	47	24	0.5	20	9	0.5	(3)			
17	1932 May 05 M				230	239	1.0	136	122	0.9	68	54	0.8				(1)															
18	1932 Sep 15 M							378			220			94	100	1.06				48	32	0.67	22	14	0.64						(3)	MM9.5
19	1934 Mar 05 M							360			220	263	1.2	111	123	1.1	75	65	0.9	62	27	0.4	35	14	0.4	(10)						
20	1934 Mar 15 M							200	160	0.8				52	48	0.9	10	10	1.0												(1)	MM7.5
21	1938 Dec 15 M				312			200	184	0.9	120	78	0.7	42	40	1	15	15	1.0												(1)	MM7.5
22	1938 Dec 16 M								460		272			112	112	1.0				(1)												
23	1942 Jun 24 M							412			256	250	0.98	136	165	1.21	73.8	79.5	1.08	45.4	34.1	0.75	(3)									
24	1942 Aug 01 M							322			163	159	0.98	107	99	0.93	62.5	57	0.91	(1)												
25	1943 Feb 17 M				455			320			180	180	1.0	90	62	0.69	(10)	(3)														
26	1943 Aug 02 M							265	200	0.75	72	100	0.72																			
27	1945 Sep 01 M							335																							(3)	MM8.5
29	1946 Jun 26 M				338			232			161						27															
30	1948 May 22 M							196	126		116	80											(2)									
31	1951 Jan 10 M							150	187	1.3				37	29	0.8															(1)	MM8.5
32	1951 Feb 10 M				250	291	1.2	187	208	1.1	110	125	1.1	50	62	1.3				(1)												

Table 2 continued:

			MM2			MM3			MM4			MM5			MM6			MM7			MM8			MM9			MM10			MM11		Misc Central Intensities	
			a	b	b/*a*	*a*	b	b/*a*	*A*	b	b/*a*	*a*	b	b/*a*	*a*	b	b/*a*	*a*	b	b/*a*	*a*	b	b/*a*	*a*	b	b/*a*	*a*	B	b/*a*	*a*	b	*a*	
34	1951	Jun	28 M						241	135	0.6	131	71	0.5				(1)														
35	1952	Aug	28 M						112	112	1.0	62	67	1.1				(1)														
36V	1953	Jul	04 V			40	40	1.0							15	15		8	8													(1)	MM7.5
36M	1953	Jul	04 M			158	158	1.0				32	32																			(1)	MM7.5
37	1956	Jan	30 V			157			120						15	15								(1)								
38	1956	Mar	02 V						27	27	1.0	12.5	12.5	1.0	7	7	1.0	(1)														
39	1957	Feb	22 M						116	83	0.7	71	37	0.5				(1)														
41	1958	Jan	31 M			269			113	113	1.0	66	55	0.8	35	24	0.7															
42	1959	May	22 M			181			125			75	87	1.2	20	20	1.0															
44	1960	May	24 M						288	288		125	108											(2)								
45	1962	Jan	23 M						179	138	0.8	58	53	0.9																		(1)	MM6.5
46	1962	May	10 M																													
47	1962	Oct	15 M						143	127	0.9	51	65					(1)														
48	1963	Apr	12 M			208			131	125	1	67	54	0.8	35	29	0.8	(1)														
49	1963	Dec	22 M									33	25	0.8	19	14	0.7	12	6.9	0.6												
50	1964	Mar	08 M						225	233	1	166	141	0.9																		(1)	MM8.5
51	1965	Apr	11 M						176	134	0.8	91									(2)												
52	1965	Jun	15 M			333			196			71	50	0.7	(1)																		
54	1966	Mar	04 M						125	150	1.2	62	65	1.05	22	22	1.0															(1)	MM6.5
55	1966	Apr	23 M						200			113	95.0	0.84	50																	(1)	MM7.5
56	1968	May	23 M						508			341			162	112	0.7	112	58	0.5	56	34	0.6	26	21	0.8	12	8	0.65			(1)	MM10.5
57	1968	Sep	25 M						300						142									(2)								
58	1968	Nov	01 M						187	204	1.1	60	87	0.7	29	29																(1)	MM6.5
59	1971	Aug	13 M						237			135	118	0.9							(1)											
60	1972	Jan	08 M						115	95	0.8	69	44	0.6	19	19	1.0	6.8	6.8	1.0												(1)	MM7.5
62	1974	Sep	20 M			316			187	137	0.7							(1)															
63	1974	Nov	05 M						240	255	1.06	120	76	0.64	50	30	0.6	(1)															
65	1975	Jun	10 M						213	168	0.89	71	50	0.7	25	21																(1)	MM6.5

Table 2 continued:

		MM2			MM3			MM4			MM5			MM6			MM7			MM8			MM9			MM10			MM11		Misc Central Intensities	
	Date & Region	*a*	b	b/*a*	*a*	b	b/*a*	*a*	b	b/*a*	*a*	b	b/*a*	*a*	b	b/*a*	*a*	b	b/*a*	*a*	b	b/*a*	*a*	b	b/*a*	*a*	b	b/*a*	*a*	b	*a*	
66	1976 May 04 M										144	108	0.8										(2)									
67	1976 Oct 27 V										18.9	21	1.1	9.5	9.2	1	3.2	2.9	0.9													
68	1976 Dec 05 M							69	65	0.9	51	46	0.9	38	29	0.8	19	14	0.7												(1)	MM7.5
69	1977 Jan 18 M							299			103	101	1				(1)															
70	1977 May 31 V							40			27	27	1.0	16	16	1.0	7	7	1.0													
71	1979 Oct 12 M											228																				
72	1982 Sep 02 M							119	152	1.3	58	86.9	1.5	(1)																		
73	1983 Dec 14 V							31.4	27.0	0.88	17	15	0.8	10.1	7.9	0.8	6.2	4.4	0.7													
75	1984 Jun 24 M										163	114	0.7	63	45	0.7															(2)	MM8.5
76	1985 Jul 19 M							145			73	58					(1)															
77V	1987 Mar 02 V							133			100			45			35			22.0	15	0.68	12	8	0.67						(2)	MM9.5
77M	1987 Mar 02 M											140			54			20			15			6						(2)	MM9.5
78	1988 Jun 03 M													174			83															
79	1989 May 31 M											163			72																	
80	1990 Feb 10 M							194						50.8	29	0.5				22	11	0.5									(1)	MM8.5
81	1990 Feb 19 M							199	224	1.1	72	72	1	43	31	0.7															(2)	MM7.5
82	1990 May 13 M							233	228	1	109	119	1.1	53	46	0.9	32	33	1	15	16.1	1										
83	1993 Apr 11 M							112	82	0.7																					(1)	MM6.5
84	1993 Aug 10 M							320	288	0.9	152	128	0.8																			
85	1993 Aug 10 M											73					27	18	0.7													
86	1994 Jun 28 M											100			62																	
88	1995 Nov 24 M					150																										
90	Dummy A*M																									(3)						
91	Dummy B*V																									(3)						

Notes: * Two dummy events, see text.

Dummy epicentral data in brackets, eg (3), see text.

Table 3: Isoseismal distance data for Deep earthquakes (km).

		MM3	MM4	MM5	MM5.5	MM6	MM6.5	MM7	MM7.5
No.	Date	a b_e b_w	a b_e b_w	a b_e b_w	a b_e b_w	a b_e b_w	a b_e b_w	a b_e b_w	a b_e b_w
6	1914 Nov 22			800		496 500 75		297 300 36	(1) (1) (1)
7	1921 Jun 28		800 220	440 400 76		158 150 52		(1) (1) (1)	
28	1946 Feb 12	420 350 230	236 200 140	(1) (1) (1)					
32	1951 Apr 23	387	278	206 190 145		116 100 73		(1) (1) (1)	
40	1957 Aug 11	290 250 102	(1) (1) (1)						
43	1960 Feb 03		297 250 100	(1) (1) (1)					
53	1965 Dec 08	778 650 202	579 500 110	(1) (1) (1)					
61	1973 Jan 05		600 200	268 250 116		117 100 45	(1) (1) (1)		
64	1975 Jan 04		237 210	133 120 70		(1) (1) (1)			
74	1984 Mar 08		420 350 129	180 150 81		(1) (1) (1)			
87	1995 Mar 22		352 290	106 90 76	(1) (1) (1)				
89	1998 Jul 09	1280					(1)		

Note: Dummy "epicentral" data, in brackets, i.e. (1), see text.

Table 4: Values of I_o and I_{ii} for the 17 shallowest earthquakes

Event No.	M_W	I_o	I_{ii}	h_t	FM
1	8.2	10.5-11	10	0	S
2	7.1	10	9	0	S
3	6.78	9.5	9	4	R
12	4.6	7	7	3	N
13	6.95	10	9	0	S
14	5.45	8	7	8	S
15	7.7	10.5-11	10	0	R
16	7.8	10.5-11	10	0	S
18	6.79	9.5		2	S
19	7.36	10		1	S
23	7.07	9	8	4	S
30	6.36	9		1	S
49	4.93	7.3	7	4	N
56	7.23	10.3-10.5	10	0	R
59	5.70	8.5		6	S
60	5.26	7.5	7	5	N
77	6.53	9.5	9	0	N
80	5.93	8.5	8	6	S

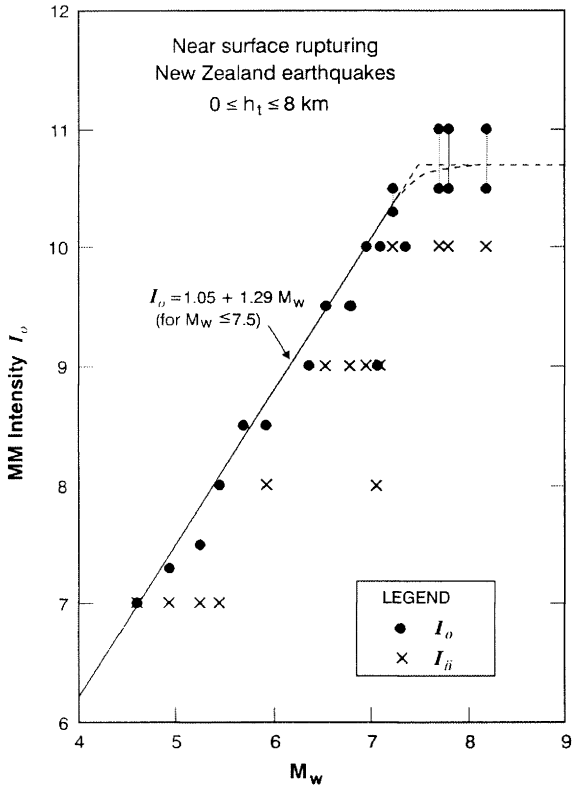

Figure 4: ***Plot of data for intensity at centre (I_o) and innermost isoseismal (I_{ii}) for near surface rupturing earthquakes, with upper bound line for I_o versus M_W.***

It is of interest to examine the values of I_o and I_{ii} for near-surface earthquakes. As listed in Table 4, there are 18 events in our database for which the depth to the top of rupture is $h_t \leq 8$ km, with a mean h_t-value of 2.4 km. The data in Table 4 are plotted in Figure 4, together with a line representing the approximate upper bound of MM intensity I_o as a function of magnitude, given by

$$I_o = 1.05 + 1.29\, M_W \quad (\text{for } M_W \leq 7.5) \qquad (2)$$

As seen in Figure 4, it appears that for very shallow earthquakes I_o is a linear function of M_W over a wide magnitude range, $4.5 \leq M_W \leq 7.5$. Saturation of intensity becomes noticeable at a magnitude of about M_W 7.5, and an intensity of nearly MM11. This suggests that intensity MM12 may never occur. See further comments on I_o (maximum) in Section 7.0.

4.0 DEVELOPMENT OF THE ATTENUATION MODELS

Attenuation models were developed for subsets of the data by applying multiple regression modelling to the MM intensity data, with moment magnitude and a function of source distance being the primary explanatory variables, but with centroid depth, tectonic region, tectonic type and focal mechanism also being considered for inclusion in the models. Models were developed for the along-strike source distance r_a using a similar approach to Dowrick and Rhoades (1999), but the treatment of the normal-to-strike direction was quite different, as described below.

The regression model used was the random effects model (Abrahamson and Youngs, 1992) in which the error variance is decomposed into a within-earthquake component σ^2 and a between-earthquake component τ^2. The enhancement of the random effects model to allow for individual earthquake magnitude uncertainties (Rhoades, 1997) was used. This model allows magnitude data of relatively low quality to be included in the analysis and given the weight that they are due. It extracts the effect of magnitude uncertainties from the between-earthquake component of variance. We divided the magnitudes into four classes of quality, A, B, C and D, for which standard errors of 0.1, 0.15, 0.3 and 0.3 respectively were adopted. The value of 0.1 for class A standard errors reflects the very small standard errors published for systematic estimates of M_W (e.g., Urhammer *et al.*, 1996). The value of 0.15 for class B is based on an estimate of Dowrick and Rhoades (1998) for this class. The value of 0.3 for class C is based on typical errors in regressions of magnitude on fault rupture length and displacement (Wells and Coppersmith, 1994; Dowrick and Rhoades, 2004). The value of 0.3 for class D is based on the authors' judgement, and has been justified by the fit of the data to the models subsequently found for the four events involved.

A new non-linear function of source distance, denoted log$D$ (meaning $\log_{10}$D) was applied in the along-strike direction regression modelling. It has the form

$$\log D = \log_{10} [(r^3 + d^3)^{1/3}] \qquad (3)$$

where $r = r_a$, and d is a parameter to be estimated. The use

of log$D$ as a regression term rather than log$r$ improved the fit to the near source intensity data, and a non-zero value of d was found to be useful for all subsets except the deep earthquakes considered by themselves. The cubic form of D in Equation (3) proved to be a useful improvement on the quadratic form normally used in attenuation functions, as in our 1999 model. It introduces necessary extra curvature into the near-source part of the attenuation curve, as shown in Figure 5(a). By relating the b-direction and a-direction using the method discussed in the next section, the relations of MM intensity against distance in the two directions plot as shown in Figure 5(b).

Indicator variables were used to include the effects of factors, such as focal mechanism, tectonic type and tectonic region, in the regression models. For a given level L of a factor F, the indicator variable δ_L is defined by $\delta_L = 1$ if $F = L$, and 0 otherwise.

5.0 DISCUSSION OF THE ATTENUATION MODELS

5.1 Functional Form

The random effects models fitted in the along-strike direction is of the form

$$I = \alpha + \beta M_W + \gamma \log D + \sum_{l=1}^{m} \theta_l x_l + \xi + \varepsilon \quad (4)$$

where, I is Modified Mercalli intensity, M_W is moment magnitude, log$D$ is as defined above, x_l, $l=1...m$ are additional regression terms, ξ is a normally distributed random variable which is determined by the earthquake and has variance $\beta^2 s^2 + \tau^2$ where s is the earthquake magnitude standard error, and ε is a normally distributed random variable with mean zero and variance σ^2. The parameters to be estimated are $d, \alpha, \beta, \gamma, \theta_l, l = 1...m, \tau$ and σ.

Models were developed for three different subsets of the data, namely:

(1) all data with known focal mechanisms, excluding only Deep events;

(2) the Main Seismic Region (all of New Zealand except the Taupo Volcanic Zone, see Figure 1), excluding Deep earthquakes;

(3) Deep earthquakes.

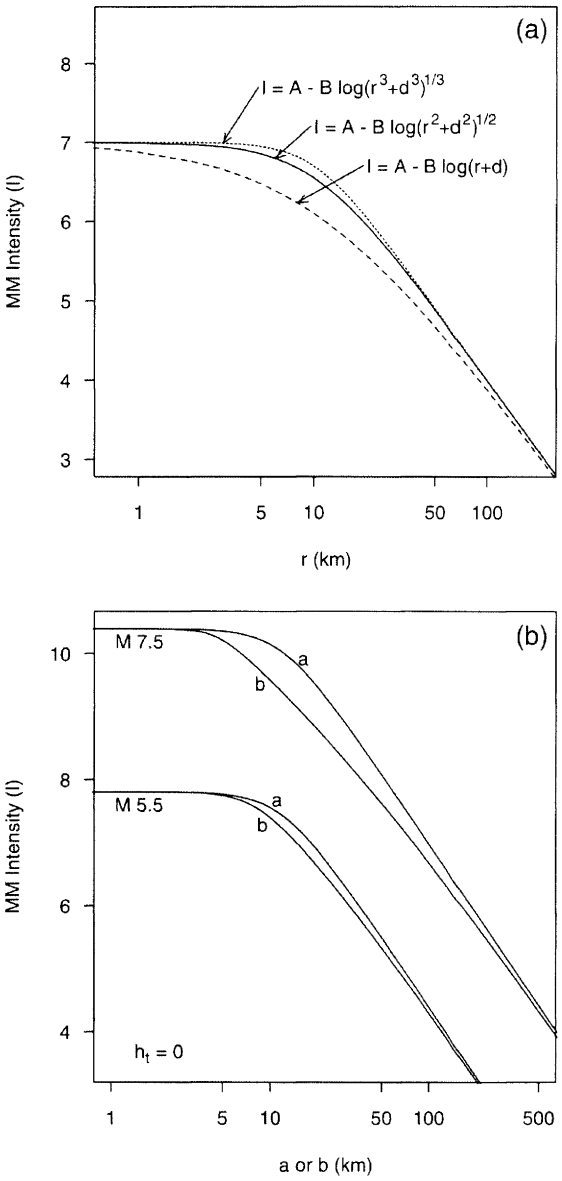

Figure 5: ***(a) Comparison of shapes of the attenuation curves derived using linear, quadratic and cubic forms of distance term. The cubic form gives the best natural control of the fit to near source data.***

(b) Plots of attenuation models for a small and a large surface rupturing earthquake showing the convergence of the a and b dimensions in the near and far fields.

The parameter estimates, standard errors, residual standard deviations, and the number of data for each model are given in Tables 5-7. For subset (3) the number of data was insufficient to give stable estimates of the error terms τ and σ. Shallow earthquake data from the main seismic region were included in the model, with a separate set of terms fitted to the non Deep earthquakes. However, only the results for the Deep events are given in Table 7, the fit to the main seismic region having been given in Table 6.

Table 5: Model 1 "Focal mechanisms".

Parameter estimates and standard errors in random effects regression models of MM Intensity (allowing for magnitude uncertainties) in the along-strike direction using only earthquakes with known mechanisms and excluding the Deep region.

$$I = A_1 + (A_2 + A_{2R}\,\delta_R + A_{2V}\,\delta_V)\,M_W + (A_3 + A_{3S}\,\delta_S + A_{3V}\,\delta_V)\,\log_{10}(r^3 + d^3)^{1/3} + A_4\,h_C + A_5\,\delta_I$$

Where, δ_R = 1 for Reverse focal mechanisms; 0 for all other events

δ_S = 1 for Strike-slip focal mechanisms; 0 for all other events

δ_V = 1 for TVZ events; 0 for all other events

δ_I = 1 for interface events; 0 for all other events

Parameter	Estimate	Std. Err.
A_1	4.74	0.40
A_2	1.23	0.07
A_{2R}	0.042	0.020
A_{2V}	0.292	0.061
A_3	-3.613	0.078
A_{3S}	0.100	0.061
A_{3V}	-1.76	0.22
A_4	0.007	0.004
A_5	-0.42	0.19
d	10.28	0.80
τ	0.21	0.02
σ	0.38	0.01
Residual s.d.	0.43	
N**	288	
N_{eq}*	74	

Notes: ** N = Number of source-to-isoseismal distance data
* N_{eq} = Number of earthquakes

Table 6: Model 2 "Main Seismic region".

Parameter estimates and standard errors in random effects regression models of MM Intensity (allowing for magnitude uncertainties) in the along-strike direction a using data from the main seismic region (including the Northwest and Fiordland sub-regions) and excluding Deep earthquakes.

$$I = A_1 + A_2\,M_W + A_3\,\log_{10}(r^3 + d^3)^{1/3} + A_4\,h_C + A_5\,\delta_C$$

where δ_C = 1 for Crustal events; 0 for all other events

Parameter	Estimate	Std. Err.
A_1	4.40	0.51
A_2	1.26	0.06
A_3	-3.67	0.08
A_4	0.012	0.005
A_5	0.409	0.113
d	11.78	0.97
τ	0.19	0.03
σ	0.39	0.02
Residual s.d.	0.43	
N**	251	
N_{eq}*	64	

Notes: ** N = Number of source-to-isoseismal distance data
* N_{eq} = number of earthquakes

Table 7: Model 3 "Deep region".

Parameter estimates and standard errors in random effects regression models of MM Intensity for the longitudinal direction a of Deep earthquakes in the subducting Pacific plate only ($h_r \geq 70$ km).

$$I = A_1 + A_2\,M_W + A_3\,\log_{10} r + A_4\,h_C$$

Parameter	Estimate	Std. Err.
A_1	3.76	1.13
A_2	1.48	0.24
A_3	-3.50	0.22
A_4	0.0031	0.0021
τ	0.27	0.13
σ	0.42	0.06
Residual s.d.	0.50	
N**	37	
N_{eq}*	12	

Notes: ** N = Number of source-to-isoseismal data
* N_{eq} = Number of earthquakes

A problem with our 1999 model was that the fits in the *a* and *b* directions were not constrained to converge to a common value when extrapolated to zero distance from the source. Here we correct this problem by fitting a linear regression model to a function of the aspect ratio *b/a*, rather than by fitting an independent regression in the *b* direction. The model is of the form

$$y = B_1 + B_2 M_W + B_3 I + B_4 \ln a . \qquad (5)$$

where

$$y = \log \frac{b/a}{1 - b/a} . (b < a) \qquad (6)$$

Although *b/a* occasionally exceeds 1 by a small margin in the actual data, *b/a* is constrained to be less than 1 in the model. Hence in applying equation (6), values of $b/a \geq 1$ were replaced by 0.99. The AIC criterion (Akaike, 1974) was used to help decide what terms to include in the regression model (5), with terms involving focal mechanism and tectonic setting being candidates. In the interests of uniformity, the same terms have been included for each data subset. In no case did the AIC criterion justify the inclusion of more than these four terms. In the case of the deep earthquake subsets, strict application of the AIC criterion would have resulted in a more parsimonious model. The fitted parameters B_i are given in Table 8.

Table 8

Parameter estimates (± standard errors) in ordinary least-squares regressions of the form

$$\log \frac{b/a}{1\text{-}b/a} = B_1 + B_2 M_w + B_3 I + B_4 \ln a$$

for subsets : (FM) – all earthquakes with known mechanisms and excluding the deep region; (MN) – earthquakes from the main seismic region, including the Northwest and Fiordland sub-regions, and excluding the deep region; (DW) – deep earthquakes, with $b = b_w$; (DE) – deep earthquakes, with $b = b_e$.

	Subset			
Parameter	**FM**	**MN**	**DW**	**DE**
B_1	4.00 (± 0.36)	3.62 (± 0.45)	2.91 (± 0.41)	-0.13 (± 0.56)
B_2	0.58 (± 0.12)	0.45 (± 0.12)	-0.06 (± 0.09)	0.32 (± 0.12)
B_3	-0.63 (± 0.07)	-0.56 (± 0.07)	-0.09 (± 0.05)	0.02 (± 0.07)
B_4	-0.72 (± 0.10)	-0.53 (± 0.10)	-0.41 (± 0.02)	-0.17 (± 0.02)

Equations (5) and (6) provide a means of directly estimating the source-to-isoseismal distance in the *b*-direction from that in the *a*-direction. Inverting equation (6), the *b* distance corresponding to any value of *a* (and associated values of M_W and *I*) is obtained from

$$\frac{b}{a} = \frac{10^{\hat{y}}}{1 + 10^{\hat{y}}} \qquad (7)$$

where $\hat{y}$ is the fitted value of the regression model (5). If *a* is unknown, it can be estimated by inverting the along-fault attenuation relation for MMI. Equation (7) must be inverted to give a means of estimating MM-intensity from *b*, and hence to evaluate the goodness-of-fit of the procedure as a means of estimating MM-intensity.

The inversion is carried out as follows. For a given value of *b*, choose an initial estimate of $\hat{a}$ (say, *b*), and calculate a corresponding estimate $\hat{I} = I(\hat{a})$ using the *a*-direction attenuation model. Hence calculate $\hat{y}$ using equation (6), with $\hat{I}$ in the place of *I* and $\hat{a}$ in place of *a*. Then solve equation (7) to get a revised estimate of $\hat{a}$. Repeat the last three steps until convergence of $\hat{a}$ and $\hat{I}$ occurs, usually within a few iterations.

The inversion of the *b*-direction model was carried out as described above, for each data subset. This allowed us to estimate the within- and between-earthquake standard deviations τ and σ in the random effects model

$$I = \hat{I} + \xi + \varepsilon$$

where ξ and ε are distributed as in equation (4). The estimation was carried out by maximum likelihood, using equation (8) of Rhoades (1997). The estimates of τ and σ are given in Table 9.

Table 9

Error parameter estimates (± standard errors) in fit of I by $\hat{I}$ in b-direction. Subsets as in Table 8.

	Subset			
Parameter	**FM**	**MN**	**DW**	**DE**
τ	0.31 (± 0.05)	0.33 (± 0.05)	0.40 (± 0.15)	0.15 (± 0.22)
σ	0.30 (± 0.02)	0.30 (± 0.02)	0.48 (± 0.08)	0.48 (± 0.08)
Residual s.d.	0.43	0.45	0.63	0.50
N**	183	159	31	31
Neq*	67	59	12	12

5.2 Goodness of fit and robustness

The residual standard deviation of the models (calculated as $(\tau^2 + \sigma^2)^{1/2}$) is typically about 0.5 units of MM Intensity (listed in Tables 5-7), with τ being consistently less than σ. A small value of the inter-event standard error τ limits the extent to which the inclusion of further variables which are functions of the earthquake source, such as focal mechanism or tectonic type, can improve the fit, because such terms can serve only to reduce τ and not σ. For comparison we note that for Models 1 and 2 the inter-event variance τ^2 is respectively 23% and 30% of the total variance $\tau^2 + \sigma^2$. These are between the corresponding proportions of variance found for the Abrahamson and Silva (1997) attenuation model (using many parameters) for peak ground acceleration, where $\tau^2/(\tau^2 + \sigma^2)$ was 35% for $M_W \leq 5$ and 15% for $M_W \geq 7$ (N. Abrahamson, pers. comm.).

The standard errors of the parameters provide insight into how well the models are determined. These values are given in Tables 5-7. Overall, along with the residual standard deviation, they show that Models 1 and 2 are more robust than Model 3, and when considered as coefficients of variation (c.o.v.), which are defined as the standard error divided by the estimate (i.e. expected value under the model), they indicate the robustness of the individual parameters. For example the least robust term in Model 1 is h_{rs}, which has c.o.v. = 0.61 (for the strike-slip distance coefficient), with the c.o.v. values for the other terms ranging down to as little as 0.022 (for log D).

One measure of the goodness of fit of the models can be gained by examining plots of the residuals against fitted variables, where the residuals are defined as the difference between the actual and fitted value of I, to test if the assumptions of linearity are approximately satisfied. This has been done exhaustively for all models and in no case is there strong evidence of a trend in the relation between residuals and fitted values of I, or between the residuals and regression variables. Examples of such residual plots are given in Figure 6. The four plots for Model 1 (Main Seismic Region) show the model fitting the data well, with the residuals spread reasonably symmetrically about zero over the full ranges of distance, magnitude and depth as well as fitted intensity. Figure 6 also shows residuals for fitted intensities in the direction of strike for the TVZ and Deep earthquakes. These plots show that these two subsets are reasonably well fitted by the respective models.

In Figure 7 are plotted the data for a and b together with the present and 1999 Model 1, for the ten largest (M_W 6.8 – 8.2) shallow earthquakes in the Main Seismic Region. The two models are seen to be quite similar, as are the residual standard deviations (r.s.d.) for the a-direction of 0.45 for the 1999 model and 0.43 for the present model. The differences between the old and new models for the a-direction arise from two changes made in the current study: (1) changing the focal mechanism of the 1931 Hawkes Bay earthquake, and (2) the introduction of the cubic distance term.

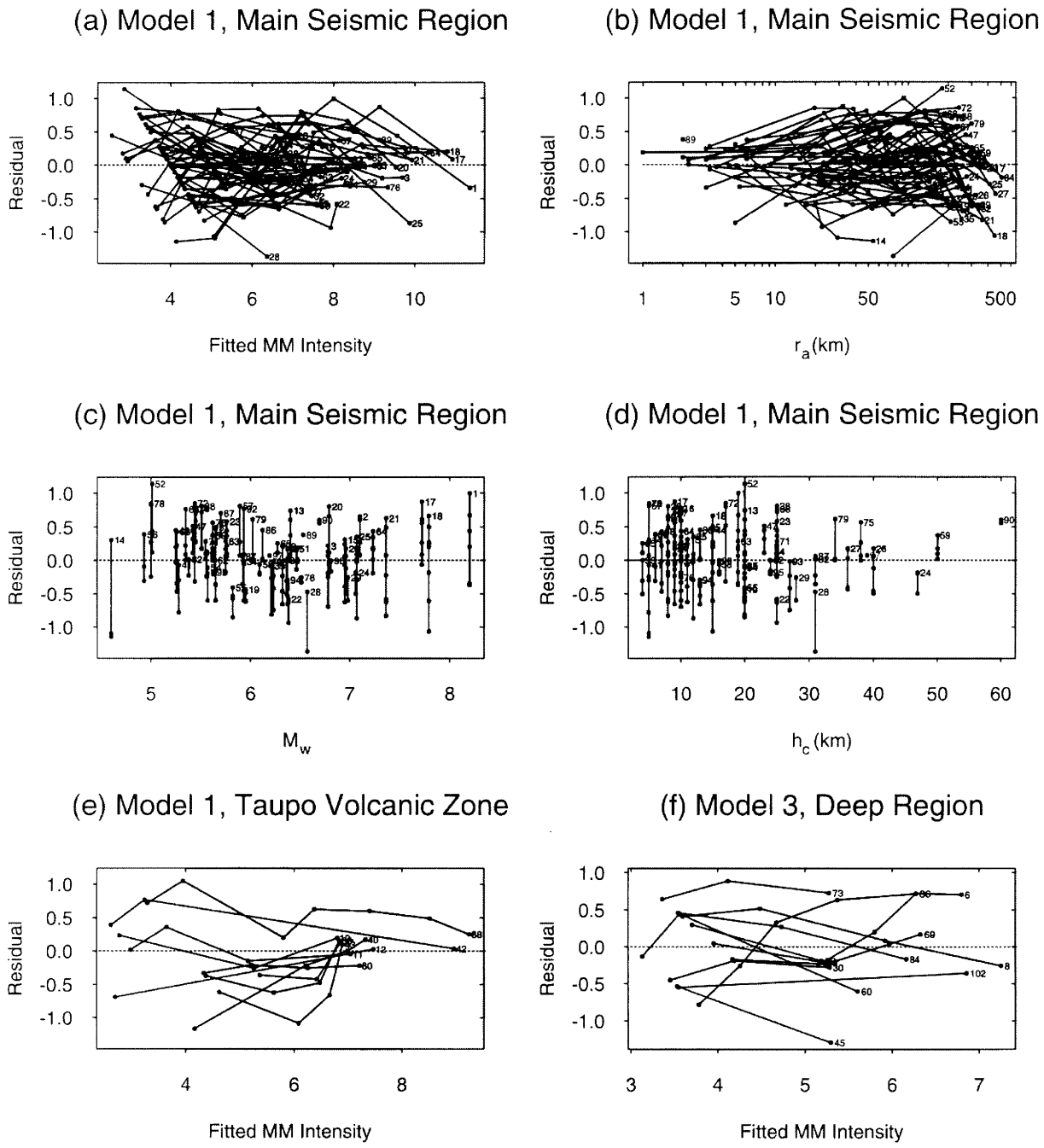

Figure 6: ***Plots of residuals for the Main Seismic Region using Model 1 (considering fitted intensity, r_a, M_W and h_c) and residuals of fitted intensities for Model 1 (for the TVZ) and for Model 3 (for Deep events).***

As well as the reduction in the r.s.d. for Model 1 noted above, a similar improvement has occurred in Model 2, with the r.s.d. being 0.43 for the present model (Table 6) as compared with 0.46 in 1999.

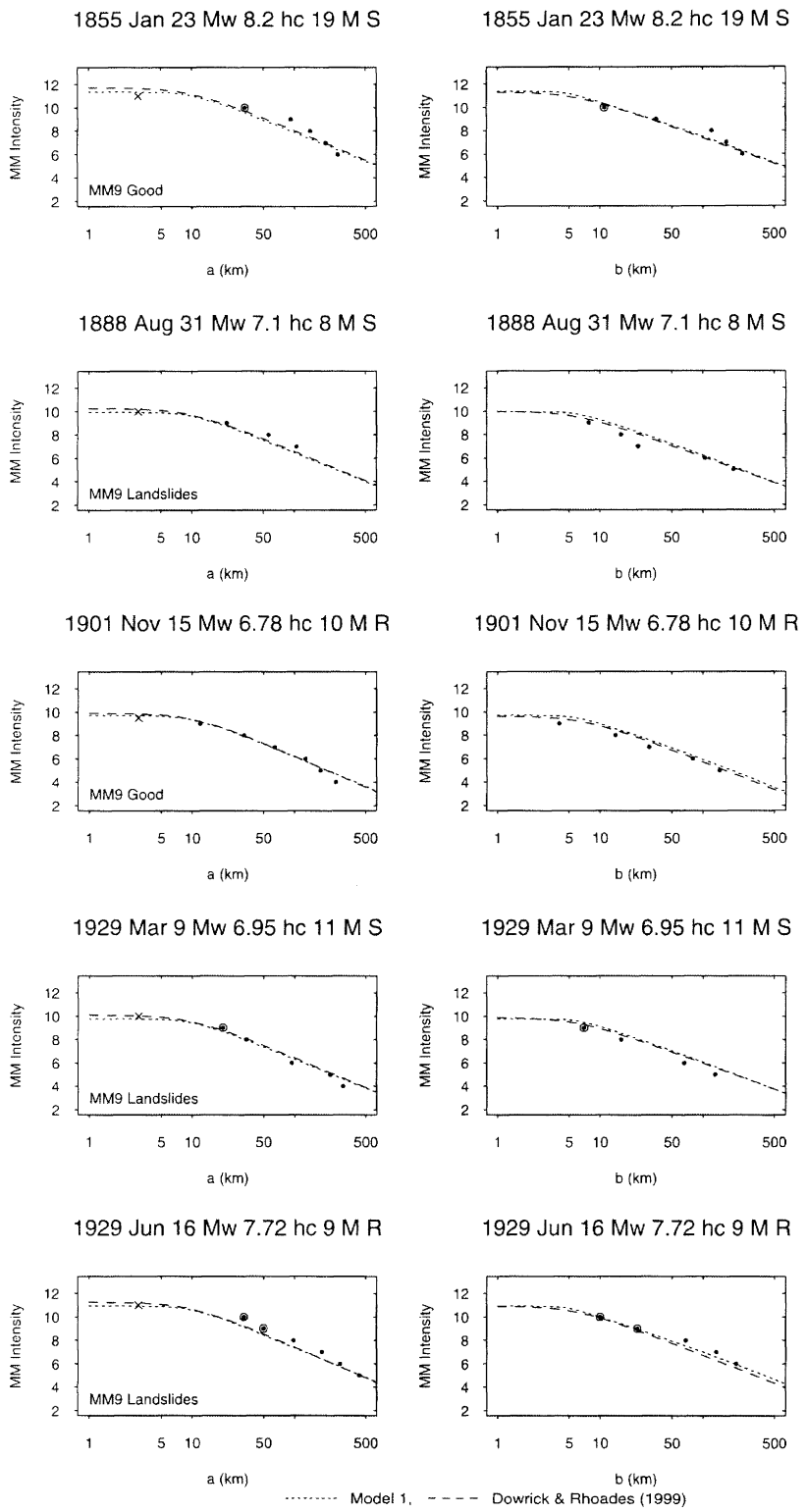

Figure 7(a): ***Plots of the 1999 and the revised Model 1 against distance a and b data for the 10 largest very shallow (7 were surface rupturing) earthquakes in the dataset, M_W 6.8-8.2, h_c 8-19 km. The header to each plot starts with the event number and ends with the region (M = Main Seismic Region) followed by the focal mechanism (R or S). For the 1855, and both 1929 events, the nearest source distance data (circled) were estimated from landslides only. Data points indicated by × are near-source controls.***

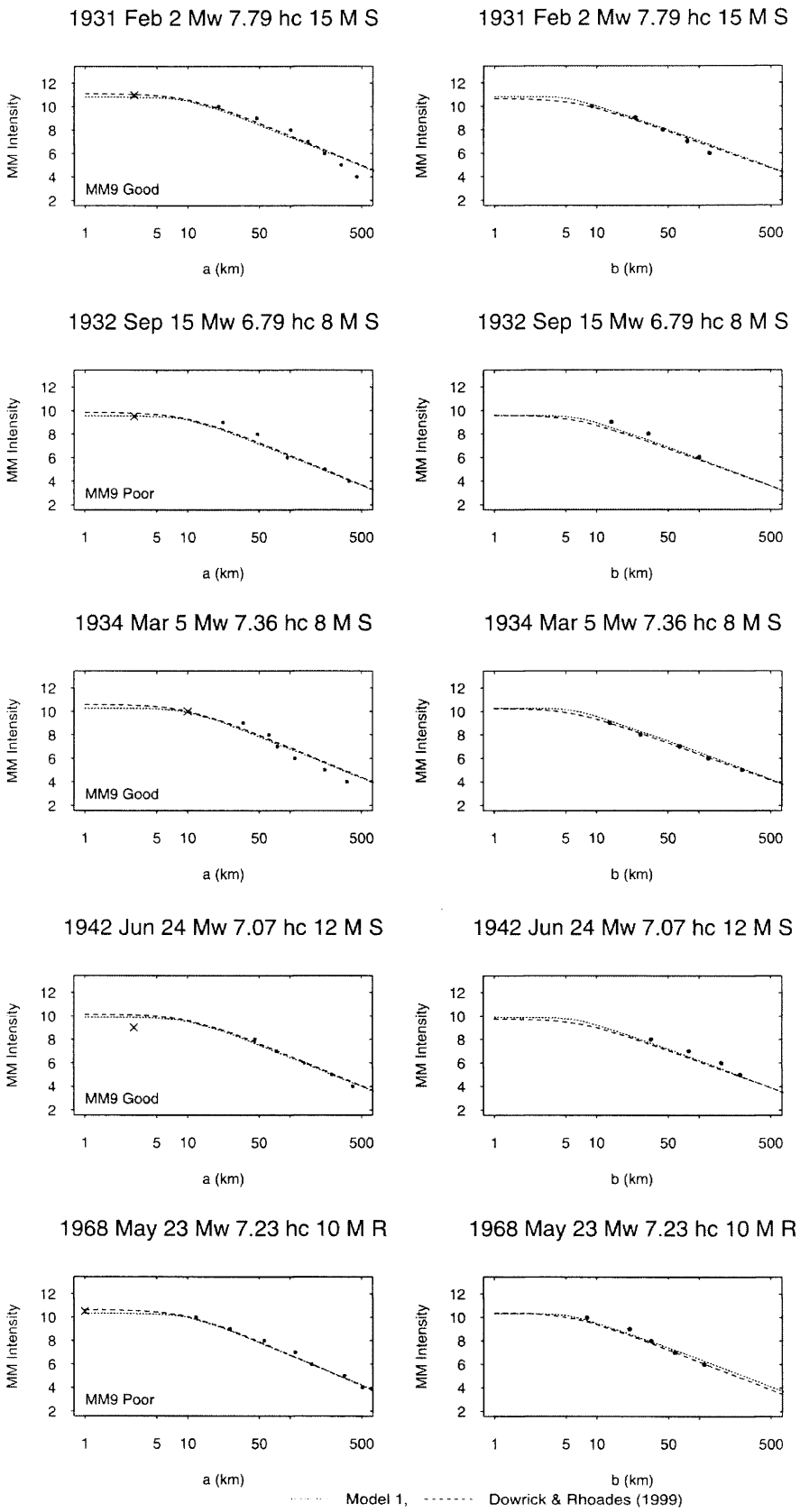

Figure 7(b): *(See caption to Figure 7(a).)*

Smith (2002) has raised concerns that our limited data for large earthquakes has resulted in a model which underestimates the along-strike dimension, a, of the inner isoseismals of some of the larger events, especially for the Murchison earthquake of 16 June 1929 (Figure 7(a)). Considering the overall good fit of the model to the data (r.s.d. = 0.43), it seems as though Smith's concern is largely based on a poor fit of the model to some poorly constrained isoseismal maps. This is illustrated by examining the control of the MM9 isoseismals on the isoseismal maps of the ten earthquakes considered in Figure 7. We have assigned them a quality level of Good, OK, Poor, or from Landslides (only), as noted on each plot. The quality levels are dependent on the number of local observations of intensity that constrain the location of the isoseismal. It is seen that five of the MM9 isoseismals are deemed to be Good or OK. The mean residual for MM9 (observed in the a-direction) is found to be 0.067, i.e. the model underestimates the intensity of MM9 by only 0.067 for these five events.

Similar plots to those shown in Figure 7 have been made for all events in the database, an examination of which shows the fit to the preferred model to be satisfactory throughout. As is consistent with the functional form of the models, there is no sign of intensity saturation effects until magnitudes of $M_W > 7.5$ and intensities approaching MM11 are reached; see the plots of 1855, 1929 June 16, and 1931 on Figure 7, and also on Figure 4. In addition, there is no sign that the attenuation rate varies with magnitude.

A limitation of all of the models is that they apply only within the range of the data used in fitting them. Outside of that range, the errors are likely to be much increased and systematic. Except for the Main Seismic Region, the range of the existing data within any particular region is quite restricted. For example, the largest magnitudes and the number (N_{eq}) of events in some of the datasets are:

- MSR Crustal M_W 8.2, N_{eq} 44 (+ Dummy M_W 7.0 Normal)
- MSR Slab (excl. Deep) M_W 7.0, N_{eq} 18
- MSR Interface M_W 6.8, N_{eq} 5
- Deep M_W 7.3, N_{eq} 12
- TVZ M_W 6.5 N_{eq} 10 (+ Dummy M_W 7.0)

For comments on the goodness of fit of Deep earthquakes to Model 3, see Section 5.7.

5.3 Effect of tectonic type

For Interface earthquakes, a negative term appears in Model 1, predicting intensities about half a unit smaller than other events of the same mechanism, M_W, h_c and source distance. This result should be viewed with caution even though Youngs *et al.*, (1997), using a large international database, found that PGAs from Interface earthquakes were weaker than those of Crustal and Slab events, for the same magnitude and distance. There are only five Interface events in our database, of M_W 5.1 – 6.8 and, after examining PGA data from Japanese Interface events, Zhao (pers. comm., 2001) says it may be that large ($M_W \geq 7$) events do not show this effect.

5.4 Effect of focal mechanism

The effects of focal mechanism on attenuation are indicated by Model 1 and are illustrated in Figure 8. It is seen that for h_c = 10 km and the same magnitude and source distance, the model predicts generally that Reverse events give higher intensities than Strike-Slip earthquakes, which in turn give higher intensities than Normal earthquakes. These effects are similar to those found in our 1999 study, and also by others using strong ground motion data (e.g. Abrahamson and Shedlock, 1997; Oglesby *et al.*, 1998; Spudich *et al.*, 1997; and Zhao *et al.*, 1997).

5.5 Isoseismal shape

As discussed in some detail in our 1999 study the mean shape of the isoseismals is a function of several parameters and varies from strongly elliptical to circular. For example, the ratio b/a at MM9 averages 0.50 for the 10 events having MM9 listed in Table 2 (these are all shallow events, having mean h_t = 0.9 km), while at MM4 b/a averages 0.95 for the 33 events with depth $h_c \leq 60$ km. The near-circular shape arises when conditions are such that the source tends to a point in size, i.e. for small magnitude and/or large distances (Figures 5(b) and 9). Some indication of this effect is also seen in Figure 10, in which are plotted the inner isoseismals of six surface-rupturing strike-slip earthquakes with magnitudes ranging from 6.7 to 7.7, together with the subsurface rupture lengths as determined using the expression of Dowrick and Rhoades (2004). In the figure it

is also seen that the innermost isoseismal does not necessarily surround the fault, as further discussed by Dowrick (2003). The shapes of isoseismals in New Zealand earthquakes can be substantially affected by the highly attenuating TVZ (Dowrick, in prep.). The data, and hence the models, are unaffected by the direction of the fault strike in relation to the predominant direction of other faults in the region (sometimes referred to as the "seismic grain" of the country).

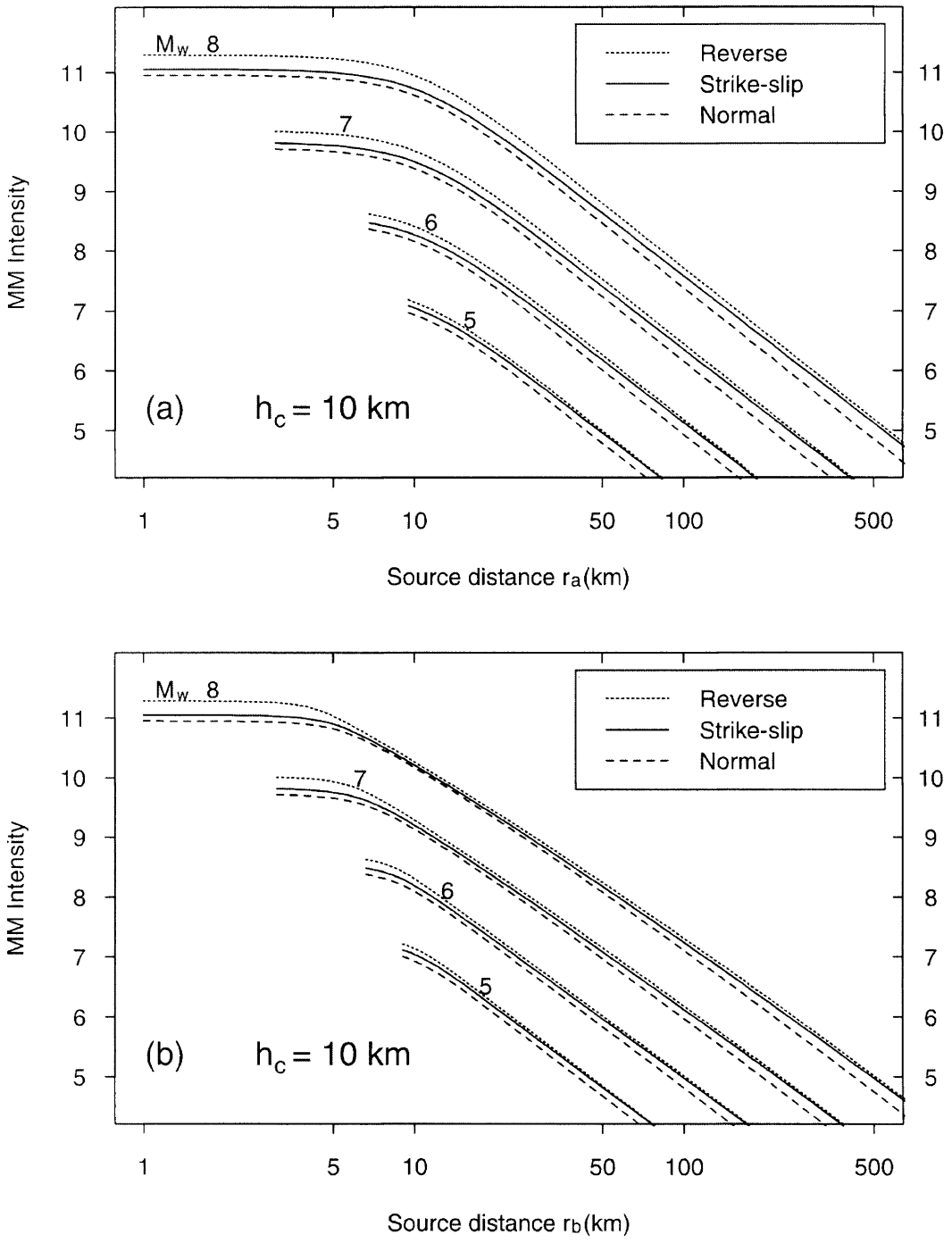

Figure 8: ***Effect of focal mechanism. Intensity plotted against source distance (a) along-strike and (b) normal to strike, as predicted by Model 1 for Strike-slip, Reverse and Normal faulting earthquakes of M_W 5, 6, 7 and 8, all of depth h_c = 10 km.***

The elliptical shapes of the isoseismals replicate (on average) the intensity patterns caused by two-dimensional sources, and imply different attenuation rates in different directions from the source.

We note that prior to our 1999 study, Chinese workers (Wang, 1988; Huo *et al.*, 1992) developed elliptical models for attenuation of MM intensity for South China, using separate regression expressions for the major and minor axes of the isoseismals, which is similar to our approach except that we use the fault strike to define the axes. Wang's South China attenuation model is further discussed in Section 7.

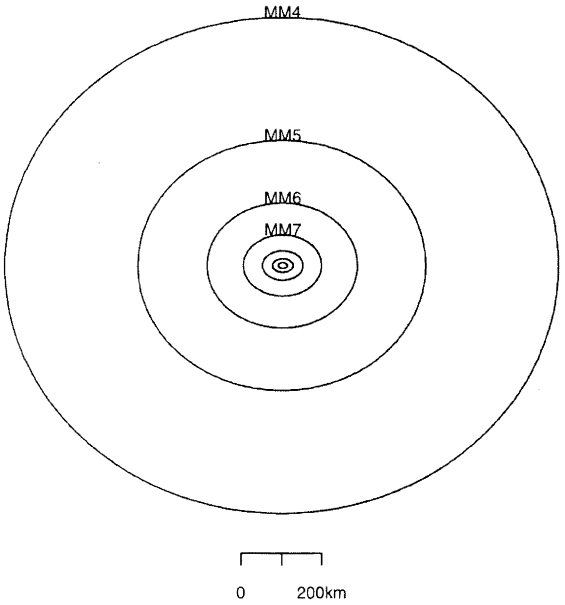

Figure 9: ***Modelled isoseismal map of a surface rupturing M_W 7.5 strike-slip New Zealand earthquake.***

5.6 Attenuation in the TVZ

The rate of attenuation in soft volcanic rock is higher than in the Main Seismic Region, as shown by the respective aspects of Model 1 (Table 5) as plotted in Figure 11. The volcanic model appears to be applicable only to travel paths within what is known as the "whole TVZ" (Taupo Volcanic Zone), the boundary of which is shown in Figure 1. This difference has been shown in various studies, e.g. for intensities in our previous study (Dowrick and Rhoades, 1999) and for peak ground accelerations by Cousins *et al.*, (1999). The volcanic model should be used with caution for larger magnitude events ($M_W \geq 7$) as there is an absence of data from such events in the present database (Table 1). In addition, the quality of the near source part of the isoseismal map for the largest volcanic region event, i.e. the M_W 6.5, 1987 Edgecumbe earthquake (No 76), is suspect (e.g. some of the intensity values are considered to be over-estimates). As seen in Figure 6(e), the intensities of this event (No. 88 in this plot) are all under-estimated substantially (and would be better fitted by the Main Seismic Region model).

It is noted that attenuation rates vary considerably within the TVZ, as discussed by Dowrick (in prep.).

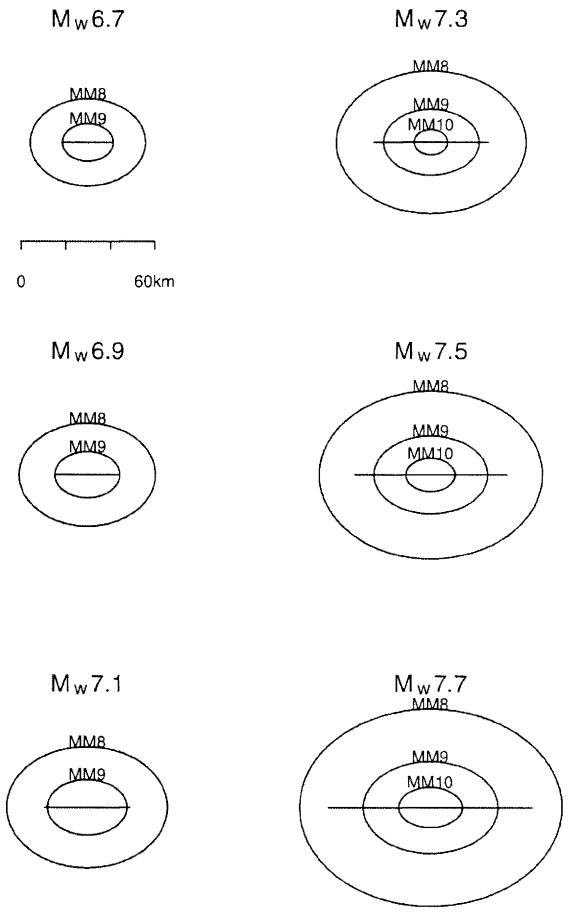

Figure 10: ***Comparison of isoseismal size and shape for surface rupturing strike-slip earthquakes of different magnitude, and hence different subsurface rupture lengths, L_{sub}, also plotted.***

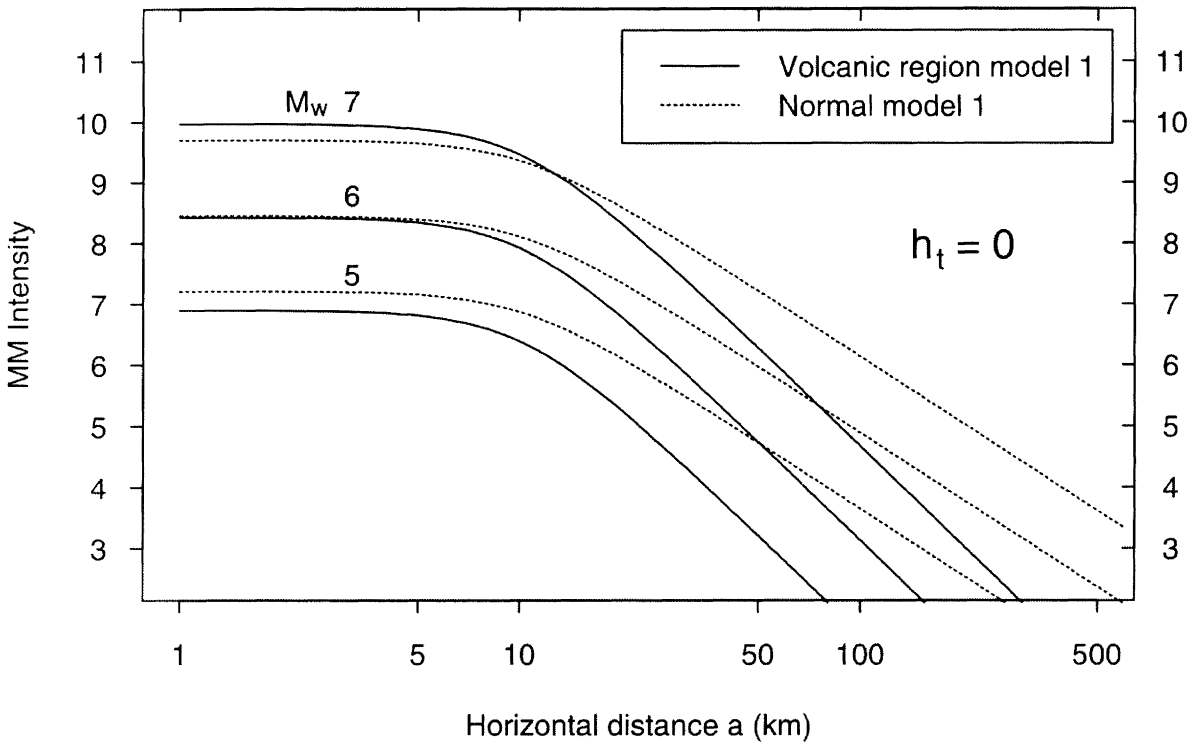

Figure 11: ***Comparison of Taupo Volcanic Zone attenuation model with that for surface rupturing Main Seismic Region Normal faulting events.***

5.7 Deep earthquakes

As discussed in our previous paper (Dowrick and Rhoades, 1999) and in Section 3 above, the effective strike of earthquakes of depth greater than 70 km is the line AA in Figure 1 which is parallel to the plate boundary. The location of such events is limited to the subducting Pacific plate which extends from about Kaikoura northwards. As shown in Figure 3, the isoseismals are asymmetrical about the line AA, such that the dimension b is larger in the easterly direction (b_e) than in the westerly direction (b_w). Our 1999 model for Deep events was deficient in that it estimated b_w but not b_e. Here models for both lateral dimensions are offered (Table 8), based on the b_w data assigned in Table 2, and the approximate b_e data assigned in Table 3.

The models for source distances in these two lateral directions of Deep events, and that for shallower slab events, are compared in Figure 12, where it is seen that the rate of attenuation for Deep events in the easterly direction is similar to that for shallow Main Seismic Region events. This result is consistent with the fact that in both cases the direct wave paths are entirely in solid rock.

While there is no event with depth in the range $61 \leq h_c \leq 69$ km in our database (Table 1), we find that the asymmetrical model for Deep Events takes over from the symmetrical one for shallow events at h_c = 70 km. This is based on the change with depth of the attenuation properties of the wave paths available to events in the subducting slab, as discussed previously (Dowrick and Rhoades, 1999). The above gap in our data has since been superseded by the recent preparation of the isoseismal map of the Marlborough earthquake of 27 May 1992, of magnitude M_w 5.9 and h_c = 67 km. Its isoseismal shapes are "symmetrical" as for the other earthquakes of h_c < 70 km.

A feature of our 1999 models was that the Deep Event Model was the poorest fitting of the three models, with an r.s.d. for the a-direction of 0.49. The new model is similar, with an r.s.d. of 0.50 (Table 7).

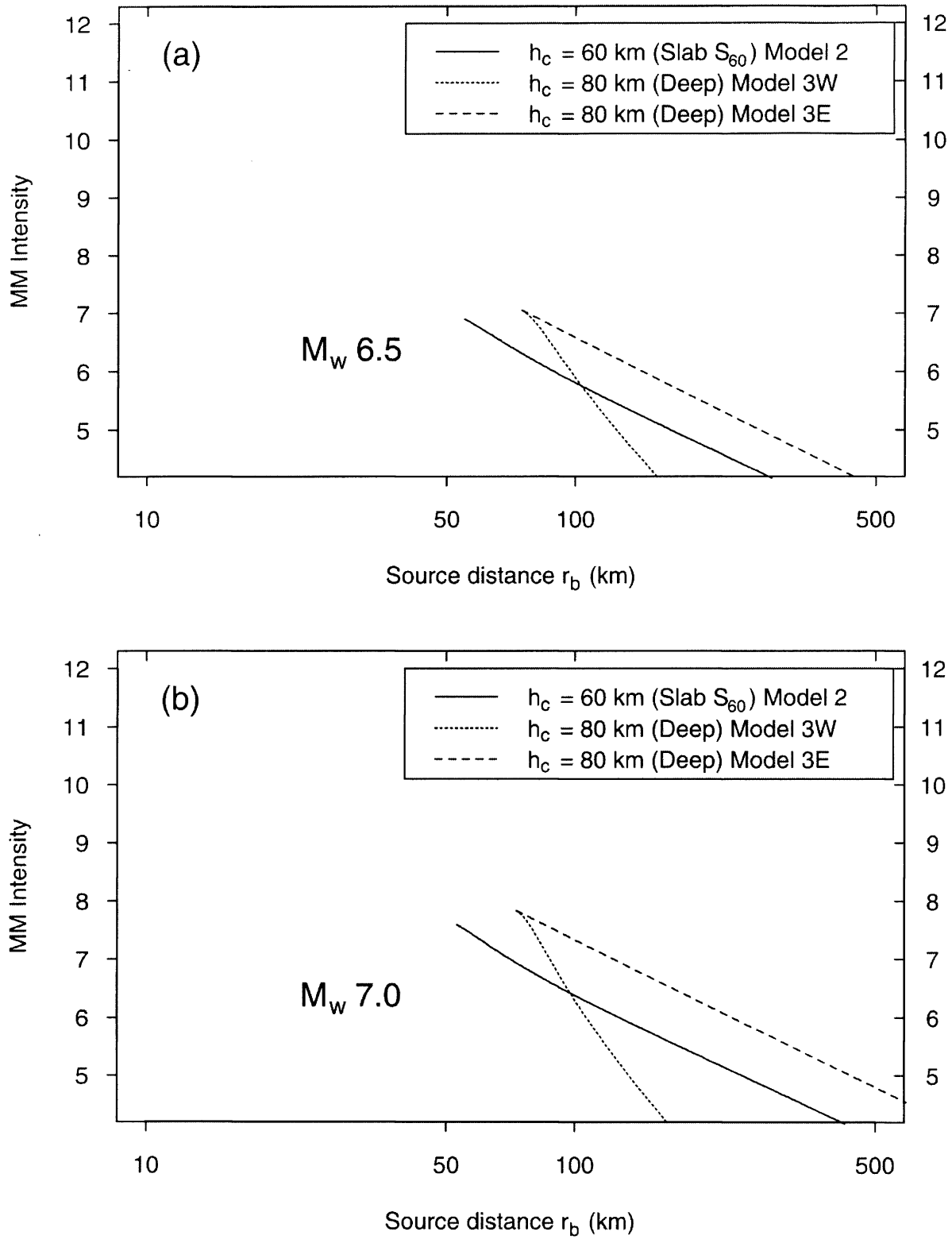

Figure 12: ***Effect of Tectonic location. Intensity plotted against lateral source distance (r_b) as predicted by Models 2, 3W and 3E for shallow Slab (S_{60}) and Deep earthquakes of (a) M_W 6.5 and (b) M_W 7.0. Note the difference in the attenuation rate between the easterly (3E) and westerly (3W) directions for the Deep earthquakes.***

5.8 Attenuation for earthquakes on long narrow fault ruptures.

In our dataset the event with the longest rupture is the M_W 8.2, 1855 Wairarapa earthquake, for which the rupture length L = 145 km (Darby and Beanland, 1992). In addition, the rupture aspect ratios length/width (L/W) of most earthquakes worldwide do not exceed about 4. Dowrick and Rhoades, (2004) discuss aspect ratios of long narrow fault ruptures for New Zealand and elsewhere. By contrast the Milford-Haupiri segment of the Alpine fault has a length of 375 km and an average width of about 11 km, so that its aspect ratio is ~34. This means that our model cannot predict the isoseismal pattern of earthquakes of M_W ~8 that are expected on that fault segment. We suggest that our model should not be used for ruptures longer than about 200 km, nor those with aspect ratios greater than about 5. Smith (2002) offers a model for very long narrow faults.

6.0 ESTIMATING SOURCE DISTANCE

The regression analyses carried out in this study were designed for the estimation of the isoseismal intensity as a function of M_W, distance D, and depth h_c, as in Equation (4). Sometimes, however, it may be desired to estimate other parameters when I is given, e.g. the source distances may be required for drawing scenario maps. A convenient way of doing that is simply to invert Equation (4) to find distance, using the appropriate parameter values given in Tables 5-7.

Thus the horizontal distance a of Figure 2 may be estimated from an expression of the form

$$a = \left[\left(10^{3(I - A_1 - A_2 M_w - A_4 h_c)/A_3} - d^3\right)^{2/3} - h_t^2 \right]^{1/2} \quad (8)$$

The above procedure involves an added approximation, because strictly speaking the parameters A_1-A_4 should be estimated from regressions of log D on I, rather than I on log D as was done for obtaining the estimates in Tables 5-7.

However, comparisons of the results obtained carrying out the two regressions, show that the estimates of I or distance are very similar. This suggests that inversions of Equation (4) may be used to estimate any of the variables without significant extra error.

7.0 COMPARISONS WITH OTHER MODELS

Attenuation Model 1 from our present and our 1999 studies are compared over a range of magnitudes for Main Seismic Region Reverse and Strike-slip events in the a and b directions in Figures 13 and 14. It is seen that for both focal mechanisms the inner isoseismals become shorter and wider in the present model than in the previous one. It is noted that both of the models for Reverse events may overestimate the intensity I_o at the centre of very shallow events of M_w c. 8+ (compare Figures 4 and 13).

In a more general sense it is of interest to examine the model for South China produced by Wang (1988), which is introduced in Section 5.5 above. The Wang models for the major and minor axes are:

$$I_a = 2.401 + 1.586\,\mathrm{M} - 1.429\,ln\,(a + 15) \quad (9)$$

$$I_b = 0.815 + 1.676\,\mathrm{M} - 1.321\,ln\,(b + 9) \quad (10)$$

The major axis model is compared with our Model 2 in Figure 15 for h_c = 10 km over a range of magnitudes. The difference in near source curvature arising from his use of a linear distance term and our cubic form as discussed in relation to Figure 5(a) above is evident in Figure 15. The deficiencies in the South China model arising from the fact that it does not allow for the source depth in the distance term are particularly apparent from the erroneously low intensities predicted for smaller magnitude events. Figure 15 also demonstrates that the South China attenuation rate beyond the near source region is considerably less than that found for New Zealand in the present study, which is consistent with differences found between attenuation rates for intraplate and interplate regions in studies of strong motion data for the USA (e.g. Atkinson and Boore, 1995).

It is also noted that the isoseismal shapes of our New Zealand models would be inappropriate for various other interplate regions where the fault rupture length for a given magnitude of earthquake differs markedly from New Zealand, such as in California where the rupture length is 50 percent longer than it is in New Zealand (Dowrick and Rhoades, 2004). This is likely to result in longer, narrower isoseismals in California than those presented here.

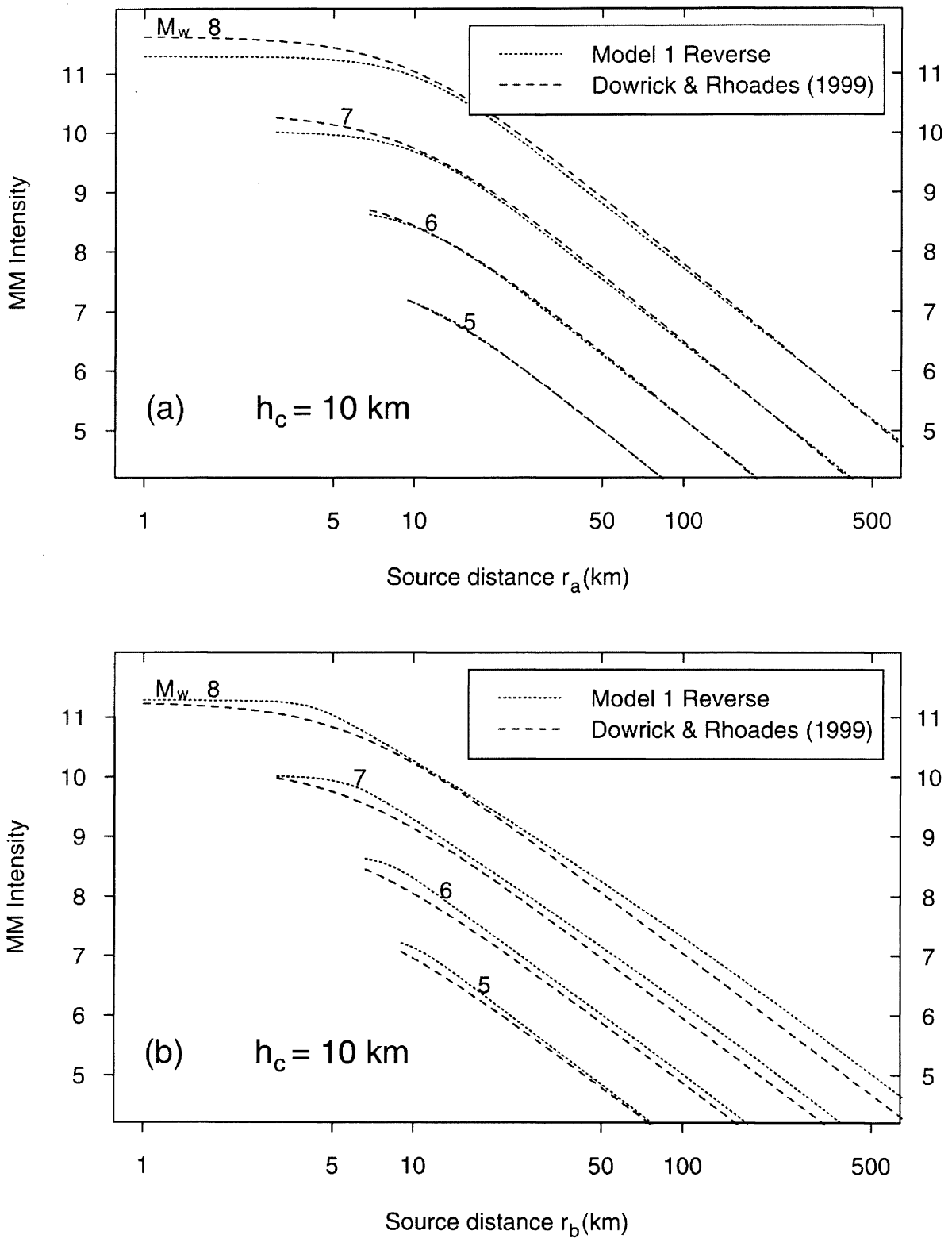

Figure 13: ***Comparison of attenuation predicted by the present Model 1 with that of Dowrick and Rhoades (1999), for Reverse focal mechanism earthquakes, (a) against distance (r_a) and (b) against (r_b).***

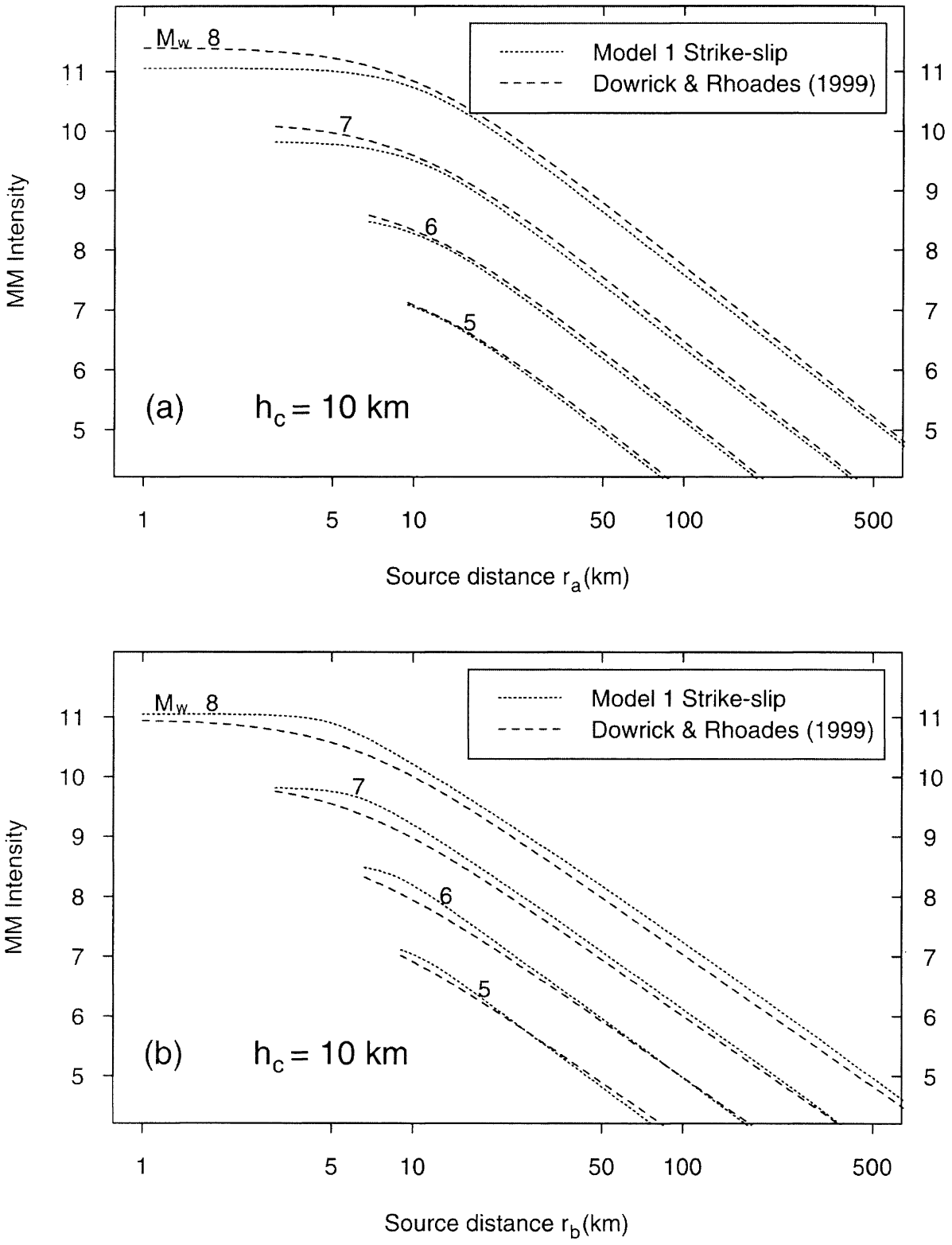

Figure 14: *Comparison of attenuation predicted by the present Model 1 with that of Dowrick and Rhoades (1999), for Strike-slip focal mechanism earthquakes, (a) against distance (r_a) and (b) against (r_b).*

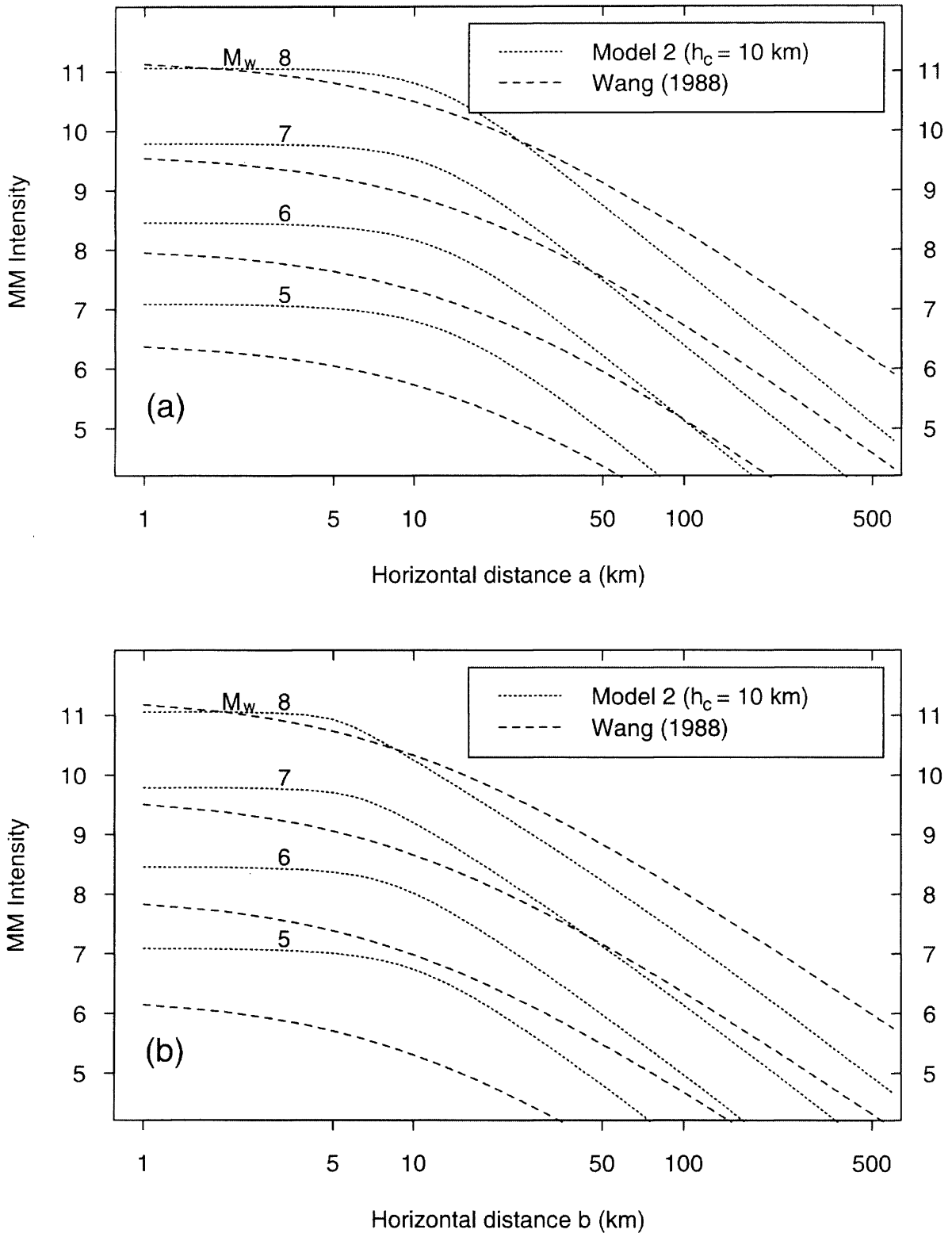

Figure 15: ***Comparison of attenuation for shallow earthquakes in the a and b directions predicted by the present Model 2 for New Zealand, with that of Wang (1988) for the intraplate region South China.***

8.0 CONCLUSIONS

As a result of this study, conclusions have been drawn as follows:

1 The new attenuation models ensure that the attenuation functions for the along-strike and normal-to-strike directions converge to the same value when extrapolated to zero distance from the source

2 A new cubic term for expressing distance, i.e. log $(r^3 + d^3)^{1/3}$ improves the modelling of the near source curvature of the attenuation function.

3 The attenuation model for Deep events ($h_c \geq 70$ km) in the subducting Pacific plate, which was incomplete in our 1999 model, has now been completed, allowing for the difference in effective attenuation in the easterly and westerly directions.

4 As found in various other studies, the model predicts that Reverse focal mechanism events give higher intensities than do Strike-slip, than do normal earthquakes.

5 The innermost isoseismal of any given earthquake does not always enclose the fault rupture.

6 Models 1 and 2 are suitable for large (M_W ~8) shallow Main Seismic Region earthquakes with small to moderate fault rupture aspect ratios L/W up to about 6, which covers most known New Zealand fault segments including the important southern segment of the Wellington fault. As such it is inappropriate for modelling events on the 375 km long Alpine fault segment which has $L/W \approx 34$.

7 Saturation of MM intensity appears to set in at $M_W >$ 7.5, and at intensities approaching MM11. This suggests that intensity MM12 may never occur.

8 The models for Reverse events may overestimate the intensity at the centre of very shallow earthquakes of M_W c. 8+.

9 The elliptical shapes of the isoseismals replicate (on average) the intensity patterns caused by two-dimensional sources, and imply different attenuation rates in different directions from the source.

10 The rate of attenuation in the far field in New Zealand (an interplate region) was found to be higher, (as expected) than that found by Wang (1988) for the intraplate region of South China.

ACKNOWLEDGMENTS

This study was funded by FRST under Contract No. C05X0209. Thanks are due to Jim Cousins, Graeme McVerry and Warwick Smith for their in-house reviews of the manuscript and also to an unknown reviewer.

REFERENCES

Abrahamson, N.A., and Youngs, R.R. (1992) "A stable algorithm analysis using the random effects model", *Bulletin Seismological Society of America,* **82**, 505-510.

Abrahamson, N. A., and Shedlock, K. M. (1997) Overview, *Seismological Research Letters,* **68(1)**, 9-233.

Abrahamson, N., and Silva, W. (1997) "Empirical response spectra attenuation relations for shallow crustal earthquakes", *Seismological Research Letters,* **68(1)**, 94-117.

Akaike, H. (1974) "A new look at the statistical model identification", *IEEE Trans. Auto. Control,* **AC-19 (6)**, 716-723.

Ansell, J., and Bannister, S. (1996) "Shallow morphology of the subducted Pacific plate along the Hikurangi margin, New Zealand", *Physics of the Earth and Planetary Interiors,* **93**, 3-20.

Atkinson, G. M., and Boore, D. M. (1995) "Ground-motion relations for eastern North America", *Bulletin of the Seismological Society of America,* **88**, 428-440.

Cousins, W. J., Zhao, J. X., and Perrin, N. D. (1999) "A model for the attenuation of peak ground acceleration in New Zealand earthquakes based on seismograph and accelerograph data", *Bulletin NZ Society for Earthquake Engineering,* **32(4)**, 193-220.

Darby, D. J., and Beanland, S. (1992) "Possible source models for the 1855 Wairarapa earthquake, New Zealand", *Journal of Geophysical Research,* **89**, 12375-89.

Doser, D.I., and Webb, T.H. (2003) "Source parameters of large historic (1917-1961) earthquakes, North Island, New Zealand", *Geophysical Journal International,* **152**, 795-832.

Downes, G. L. (1995) "Atlas of isoseismal maps of New Zealand", *Monograph 11,* Institute of Geological &

Nuclear Sciences, Lower Hutt, New Zealand.

Downes, G. L., Dowrick D. J., Van Dissen, R. J., Taber, J. J., Hancox, G. T., and Smith, E. G. C. (2001) "The 1942 Wairarapa, New Zealand, earthquakes: analysis of observational and instrumental data", *Bulletin NZ Society for Earthquake Engineering,* **34(2)**, 125-157.

Dowrick, D.J. (1992) "Attenuation of Modified Mercalli intensity in New Zealand earthquakes", *Earthquake Engineering and Structural Dynamics,* **21(3)**, 181-196.

Dowrick, D.J. (2003) "Earthquake risk reduction", John Wiley & Sons, Chichester.

Dowrick, D.J. (in prep.) "Effects of Taupo Volcanic Zone on earthquake attenuation patterns".

Dowrick, D. J., and Rhoades, D. A. (1998) "Magnitudes of New Zealand earthquakes", *Bulletin NZ National Society for Earthquake Engineering,* **31(4)**, 260-280.

Dowrick, D. J., and Rhoades, D. A. (1999) "Attenuation of Modified Mercalli intensity in New Zealand earthquakes", *Bulletin NZ Society for Earthquake Engineering,* **32(2)**, 55-89.

Dowrick, D. J., and Rhoades, D. A. (2004) "Relations between earthquake magnitude and rupture dimensions – How regionally variable are they?", *Bulletin Seismological Society of America,* **94(3),** 776-788.

Huo, J., Hu, Y., and Feng, Q. (1992) "Study on estimation of ground motion from seismic intensity", *Earthquake Engineering and Engineering Vibration,* **12(3)**, 1-15 (in Chinese).

Oglesby, D. D., Archuleta, R. J., and Nielsen, S. B. (1998) "Earthquakes on dipping faults: The effects of broken symmetry", *Science,* **280**, 15 May, 1055-1059.

Rhoades, D. A. (1997) "Estimation of attenuation relations for strong-motion data allowing for individual earthquake magnitude uncertainties", *Bulletin of the Seismological Society of America,* **87**, 1674-1678.

Spudich, P., and 10 others (1997) "SEA96 - A new predictive relation for earthquake ground motions in extensional tectonic regimes", *Seismological Research Letters,* **68(1)**, 190-198.

Smith, W. D. (1995) "A development in modelling of far-field intensities for New Zealand earthquakes", *Bulletin NZ National Society for Earthquake Engineering,* **28(3)**, 196-217.

Smith, W.D. (2002) "A model for MM intensities near large earthquakes", *Bulletin NZ Society for Earthquake Engineering,* **35(2)**, 96-107.

Stirling, M., Yetton, M., Pettinga, J., Berryman, K., and Downes, G. (1999) "Probabilistic seismic hazard assessment and earthquake scenarios for the Canterbury Region, and historic earthquakes in Christchurch", Report prepared by the Institute of Geological and Nuclear Sciences for Canterbury Regional Sciences.

Uhrhammer, R. A., Loper, S. J., and Romanowicz, B. (1996) "Determinations of local magnitude using BDSN Broadband Records", *Bulletin of the Seismological Society of America,* **86**, 1314-1330.

Wang, S. Y. (1988) "The earthquake intensity attenuation model prediction for South China region", *Earthquake Engineering and Engineering Vibration* **8(6)**, 86-97 (in Chinese).

Wells, D. L., and Coppersmith, K. J. (1994) "New empirical relations among magnitude, rupture length, rupture width, rupture area, and surface displacement", *Bulletin of the Seismological Society of America,* **84**, 974-1002.

Youngs, R. R., Chiou, S. -J., Silva, W. J., and Humphrey, J. R. (1997) "Strong ground motion attenuation relations for subduction zone earthquakes", *Seismological Research Letters,* **68(1)**, 58-73.

Zhao, J. X., Dowrick, D. J., and McVerry, G. H. (1997) "Attenuation of peak ground accelerations in New Zealand earthquakes", *Bulletin NZ National Society for Earthquake Engineering,* **30(2)**, 133-158.